Report

2006 Annual WAMIT Consortium Meeting

October 11-12, 2006

Woods Hole, Massachusetts

Agenda for 2006 Annual WAMIT Meeting
Room 310, Marine Resource Center, Swope Center, Woods Hole, MA

October 11. 2006:

9:00AM: Welcome

9:10AM: "Review of WAMIT V6.3"
C.-H. Lee, WAMIT

9:50AM: "Use of control surface option for mean drift forces"
C.-H. Lee, WAMIT

10:20AM: "Radiated wave field from a bank of wavemakers"
J. N. Newman, WAMIT

10:40AM: Break

11:00AM: "Evaluation of quadratic forces in bi-chromatic waves using control surfaces"
C.-H., WAMIT

11:30AM: "Progress for WAMIT V6.3S"
C.-H., WAMIT

12:00PM: Lunch

1:30PM: "On the numerical challenges related to side-by-side offloading and sloshing"
P. Teigen, Statoil and J.M. Niedzwecki, OTRC

2:15PM: "ATP Two Body Hydrodynamic Testing of Side-by-side Barge and Ship Models at the OTRC"
J.M. Niedzwecki, P. Teigen, R.S. Mercier & A.S. Duggal

3:00 PM: Break

3:30 PM: Technical discussion

5:30PM: Mixer and Dinner

October 12, 2006:

9:00AM: “Using WAMIT with trimmed waterlines”
J. N. Newman, WAMIT

9: 40AM: “MultiSurf developments pertinent to Wamit analysis”
J. S. Letcher, AeroHydro

10:30AM: Break

10:50AM: Business meeting

12:00AM: Lunch

Contents

Review of WAMIT Version 6.3

1 Control surface option for mean drift force

All six components of the mean drift forces and moments, on a single body or on each body in the multiple body interaction, are evaluated from the momentum flux through the control surface surrounding each body. The computational results are more robust than the pressure integration when the body surface is not smooth, especially for bodies with sharp corners.

(details in a separate presentation below)

2 Paddle wavemakers

A special option can be used to efficiently analyze the wave field generated by one or more wavemakers situated in planes of symmetry. (details in a separate presentation below)

3 Vertical hinge modes:

The DLL library file NEWMODES has been extended to include generalized mode to represent vertical modes of a vessel with hinges. (Details in Newman 1998, “Wave effects on hinged bodies. Part 1-4”)

Application may include the deck supported by vessels with hinges (right) as well as vessels connected by hinges (left).

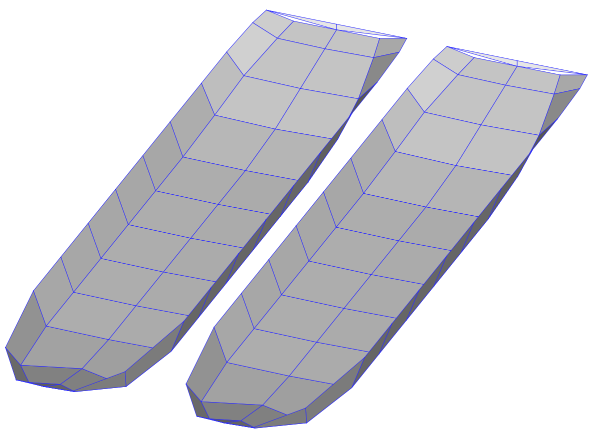

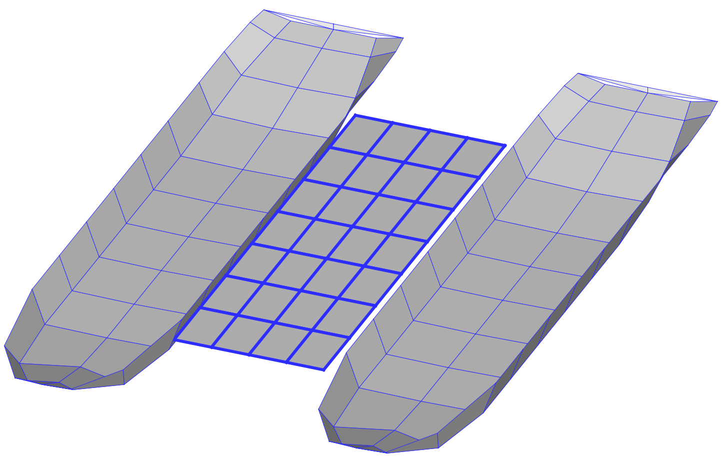

Use of option of vertical hinged modes:

a) All vessels and structures are considered as one body. One GDF describes all wetted surface.

b) In addition to 6 rigid body modes, additional modes as many as the number of the hinges (NEWMDS) are considered. NEWMDS should be specified in POT file.

c) XHINGE.DAT (in the directory the program is running)

Header (description of the file)
ISX, NSEG (symmetry index about x=0, number of segments = number of hinges + 1)
XH array (x coordinates of lower and upper limits of each segments)

When ISX=0, XH contains the x coordinates of the hinges and the lower and upper limits of x coordinates of the body surface in ascending order.

When ISX=1, x coordinates of the hinges on the positive side of x axis and the upper limit x coordinate of the should be specified in XH array in ascending order.

(Hinge axis is assumed to be parallel to y axis of the body coordinates system. In order to change this convention, user must modify NEWMODES.)

d) Mass matrix in FRC.

The inertia associated with vertical hinge modes can be evaluated from the integral in **x** of the product of

$$m(x)\ Z_i(x)\ Z_k\ (x)$$

$m(x)$ is sectional mass and $Z_i(x)$ is vertical displacement representing the shape of the hinge modes or vertical displacement of rigid body modes (heave and pitch) at x.

The products among the hinge modes and the products between hinge modes and rigid modes should be evaluated in this manner. This is to be combined with the inertia for the rigid modes (6x6) to have the complete mass matrix in FRC.

In NEWMODES, the hinge modes are described in the sequence shown below. All hinge modes have unit vertical displacement ($|Z_i(x)| <= 1$) in NEWMODES .

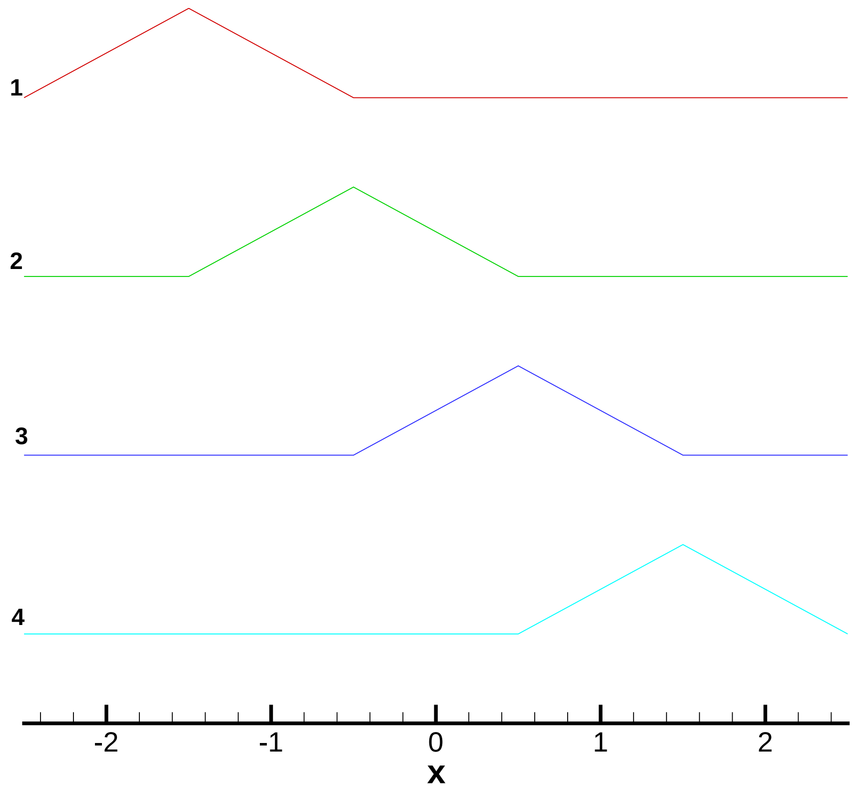

XHINGE.DAT

4 hinges & NSEG=5, ISX=0, NEWMDS=4

0 5   (ISX, NSEG)

-2.5 -1.5 -0.5 0.5 1.5 2.5 (XH)

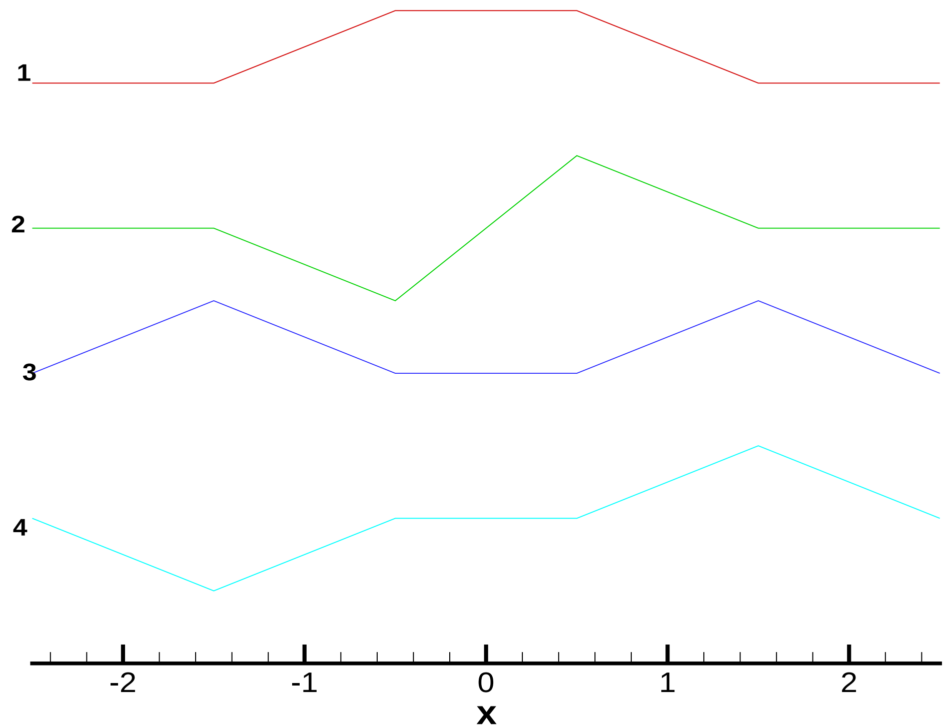

XHINGE.DAT

4 hinges & NSEG=5, ISX=1, NEWMDS=4

1 5   (ISX, NSEG)

0.5 1.5 2.5 (XH)

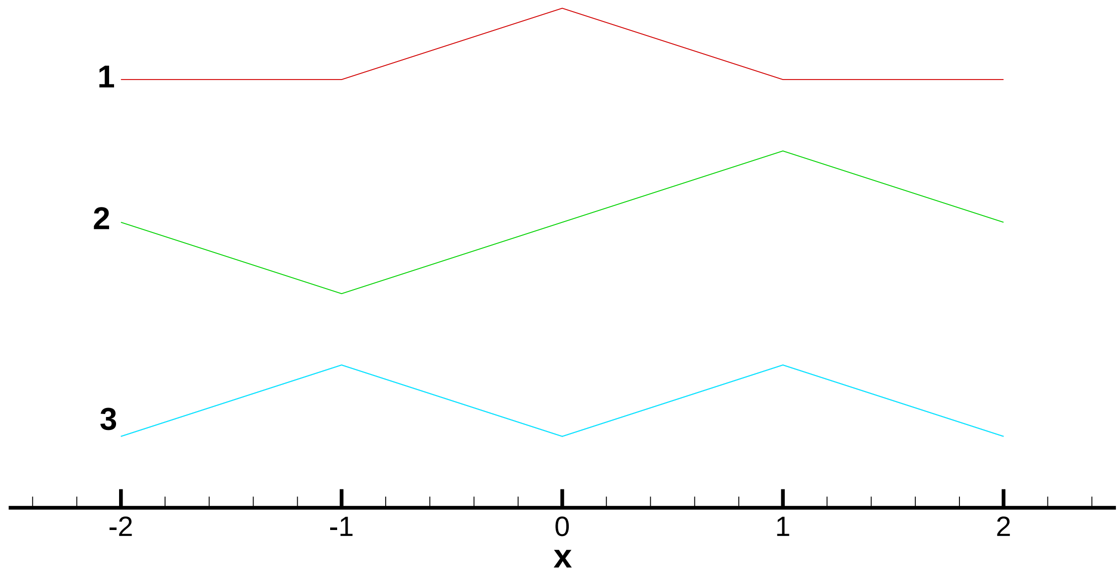

XHINGE.DAT

3 hinges & NSEG=4, ISX=1, NEWMDS=3

1 4 (ISX, NSEG)

1 2 (XH)

4 Hydrostatic coefficients matrix:

A supplementary HST output file is created to output the hydrostatic matrix of restoring coefficients, including generalized modes.

When internal tanks are present, the effect of the internal tanks is included in the hydrostatic coefficient output. These output can be used with the hydrodynamic coefficients, which also include the effect of the internal tanks, for the motion analysis outside WAMIT.

As in previous versions, the hydrostatic matrix of restoring coefficients of rigid body modes of the hull, without the effect of the internal tanks, are output, along with the some components of the hydrostatic coefficients of the internal tanks, in OUT file.

5 Uniform arrays of field points can be input in a more convenient manner.

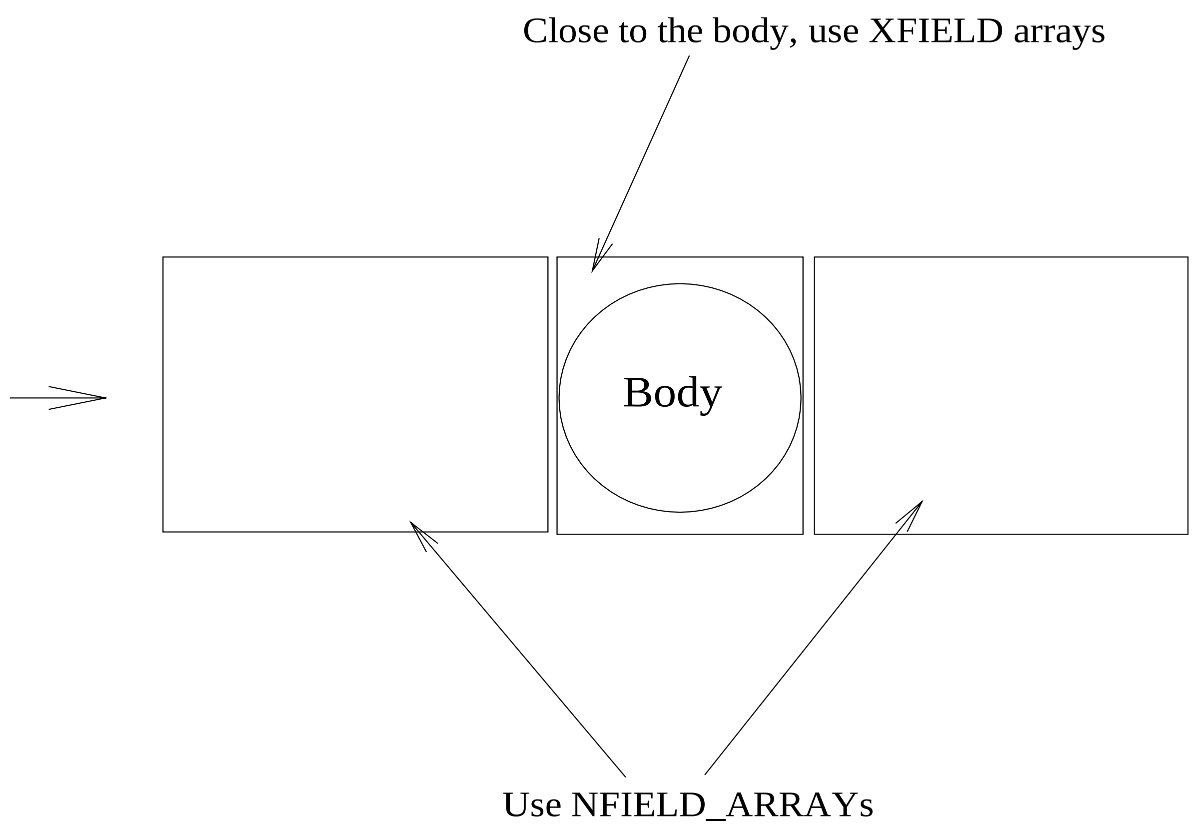

FRC (Force control file)

```
.
NFIELD
XFIELD(1,1)   XFIELD(2,1)   XFIELD(3,1)
XFIELD(1,2)   XFIELD(2,2)   XFIELD(3,2)
.
XFIELD(1,NFIELD)   XFIELD(2,NFIELD)   XFIELD(3,NFIELD)

NFIELD_ARRAYS

ITANKFLD(1)
NFX(1)  X1(1)  DELX(1)
NFY(1)  Y1(1)  DELY(1)
NFZ(1)  Z1(1)  DELZ(1)

ITANKFLD(2)
NFX(2)  X1(2)  DELX(2)
NFY(2)  Y1(2)  DELY(2)
NFZ(2)  Z1(2)  DELZ(2)

.
.
```

6 A symmetry plane can be used when there are flat dipole elements on the plane of symmetry for more efficient computation. (Example below shows the required geometric data, for a cylinder with fins on x=0 and y=0 axis.)

V6.3

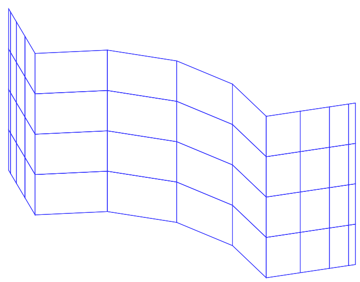

ISX=1, ISY=1

V6.2

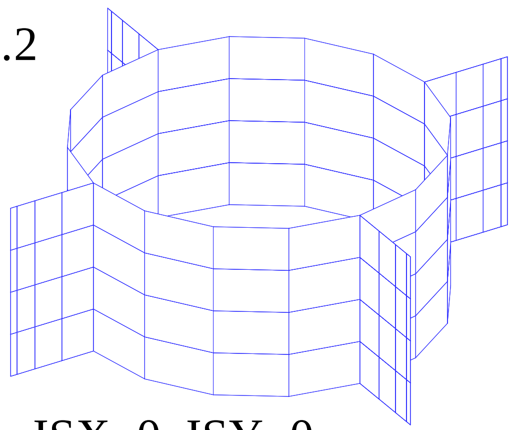

ISX=0, ISY=0

7 The DLL library file GEOMXACT has been extended to include several new analytical geometries for GDF (body geometry) and CSF (control surface).

Errors fixed in Version 6.3:

- When IPNLBPT/=0 for symmetric body, the pressure/velocity on reflected quadrants or half can be incorrect and the pressure mean drift forces can be incorrect.
- When IPNLBPT/=0, pressure can be incorrect when the points are near the intersection of normal and dipole panels when low-order method is used.
- Hydrostatic restoring force due to internal tank can be incorrect. This affects, RAO, body/field pressure/velocity and mean forces.
- The fluid velocity on tank wall is incorrect when IDIFF>-1 in low-order method. This also affects pressure mean drift forces.
- The pressure mean drift forces/moments in heave, roll and pitch are incorrect when the vertical positions of tank free surfaces are different from the free surface.
- The output may be incorrect with the presence of tanks in the low-order method when IRR=2 option is used
- Impulse response functions for the radiation pressure/velocity on the body and field points are not correctly evaluated in F2T.

Use of control surface option for mean drift forces

In V6.3, the mean drift forces can be evaluated from the momentum flux through a control surface surrounding each body. The preparation of input and the use of this option is described below.

1. New input parameters and output file
2. CSF (control surface file)
3. Alternatives 1 and 2
4. Example 1 – sphere & cylinder
5. Example 2 – barge created by MultiSurf (test20)
6. Example 3 – body with non-vertical wall
7. Example 4 – body with dipole element
8. Summary

1. New input parameters and output file

INPUT:

a) ICTRSURF=1 or ICTRSURF=2 should be specified in Configuration file (CFG). ICTRSURF specifies one of two Alternatives for integrating the momentum flux over the control surface

b) IOPTEN(9) > 0 in Force control file (FRC)

c) The surface geometry of the control surface should be input in a file with the filename same as GDF and extension CSF (gdf.CSF).

OUTPUT:

The mean forces using control surface are output in IOPTN.9c

The pressure mean forces are output in IOPTN.9

2. CSF (control surface file)

CSF describes the control surface surrounding each body. The format of the file is similar to GDF (all of the geometry definitions in GDF can be used in CSF).

Low order format:

GDF:	CSF:
Header	Header
ULEN GRAV	0 (ILOWHICSF)
ISX ISY	ISXCSF ISYCSF
NEQN	NEQN
XVER array	XVER array

Higher order format

GDF:	CSF:
Header	Header
ULEN GRAV	1 (ILOWHICSF)
ISX ISY	ISXCSF ISYCSF
NPATCH IGDEF	NPATCSF ICDEF PSZCSF

a) control surface includes the free surface and SC and SF are input in CSF. CL and WL are found in WAMIT and are not part of the input.

b) the convention for normal vector is the same in CSF and GDF. Panel vertices are in counter -clockwise direction for ILOWHICSF=0 and the normal vector points inward for ILOWHICSF=1.

c) arbitrary combination of ILOWHI and ILOWHCSF can be used. (ILOWHI=0 and ILOWHICSF=1 is ok. But the intersection between body and free surface may be inaccurately described.

d) horizontal forces and yaw moment can be evaluated without free surface in alternative 1 method and the intersection problem in c) is not a concern

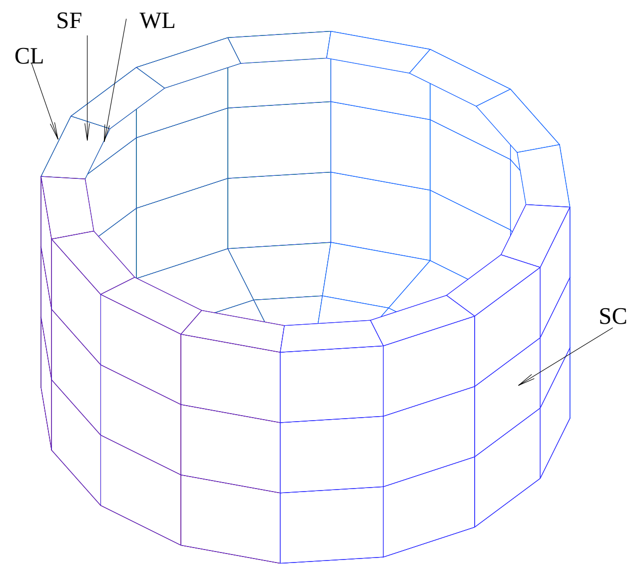

Alternatives 1 and 2

A) For horizontal momentum (surge, sway, yaw)

Two alternatives are equivalent but different in the way to evaluate momentum on the free surface. In alternative 1, the horizontal momentum is evaluated only on CL, while in alternative 2 on SF and WL. Robust evaluation of momentum on SF near the waterline and WL requires more refined description on the body near the waterline and less efficient than the evaluation on CL.

B) For vertical momentum (heave, roll, pitch)

Two alternatives are identical and require SF in CSF.

Alternative 1 should be used in most cases: a) more efficient b) SF not required in CSF for the horizontal momentum. Alternative 2 option may be used for such exceptional case as two vessels with a lid in-between. Without no or little gap between the body and CL, as shown below, Alternative 1 can not be applied.

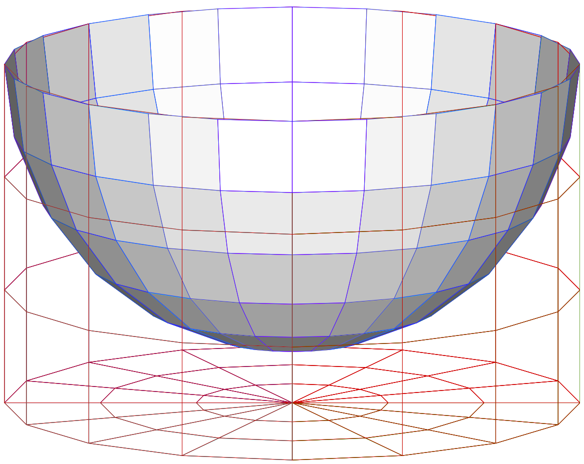

Example 1 – sphere & cylinder

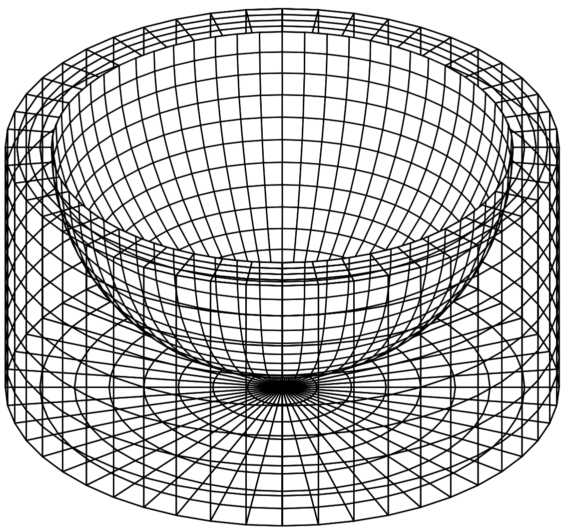

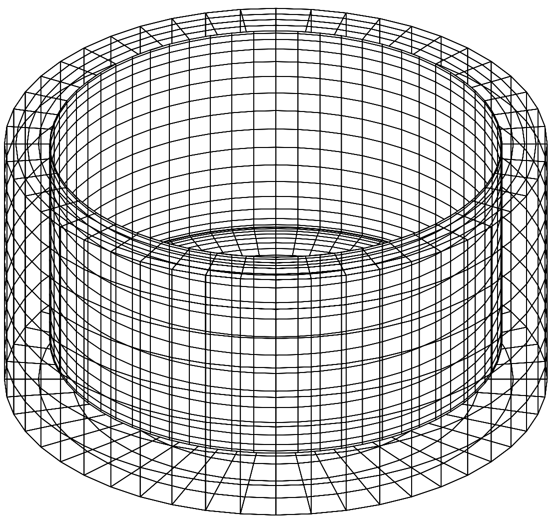

Computed by higher-order method

1, 4, 16 panels on the sphere
2, 8, 32 panels on the cylinder

1, 4, 16 panels on the interior free surface

Solid Line: Momentum
Dotted Line: Pressure
Square: Control Surface

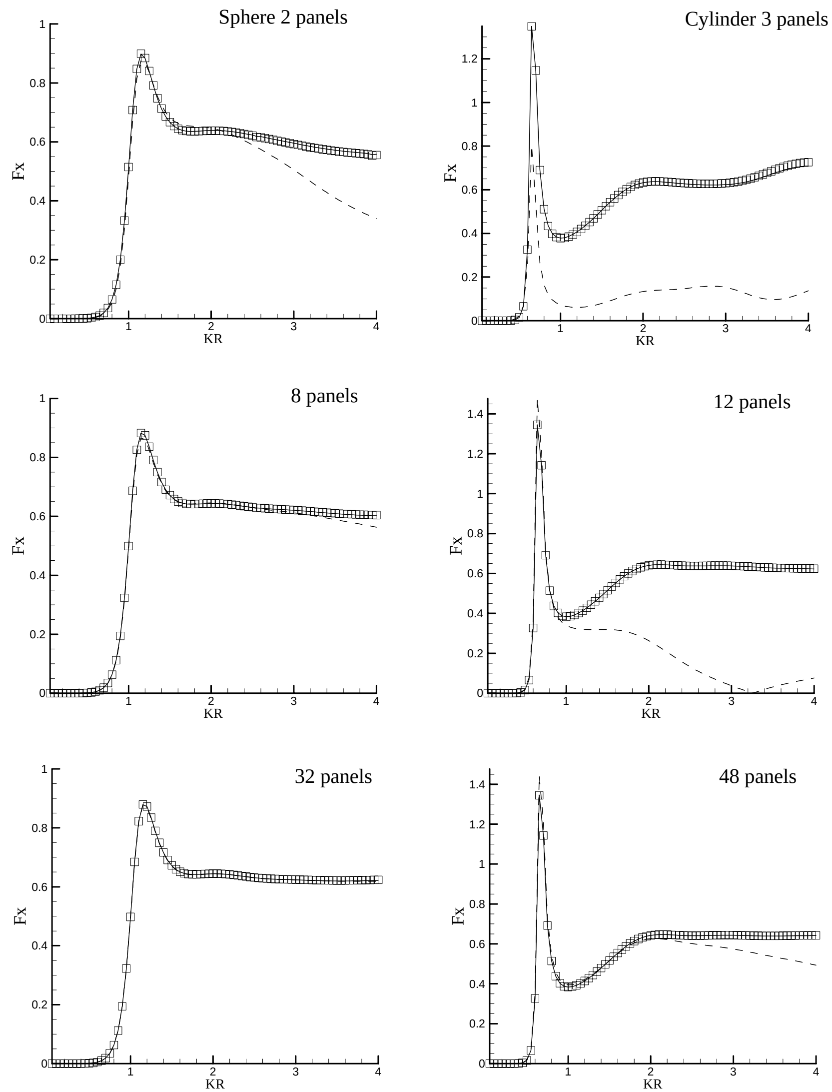

Sphere Cylinder

With no gap between CL and WL, alternative 2 must be used.

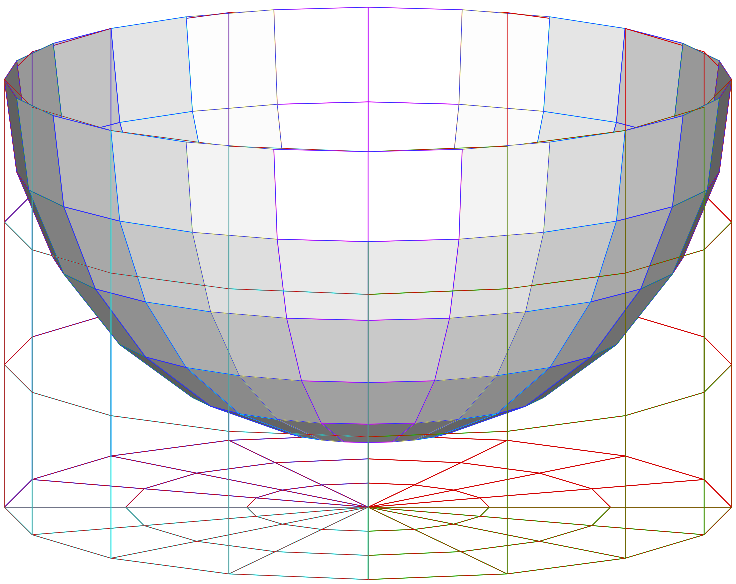

Alternative 2 method for a sphere.
Results suggest more refined soltuion on the body near the waterline
for accurate evalutation of the flux on the control surface near the waterline.

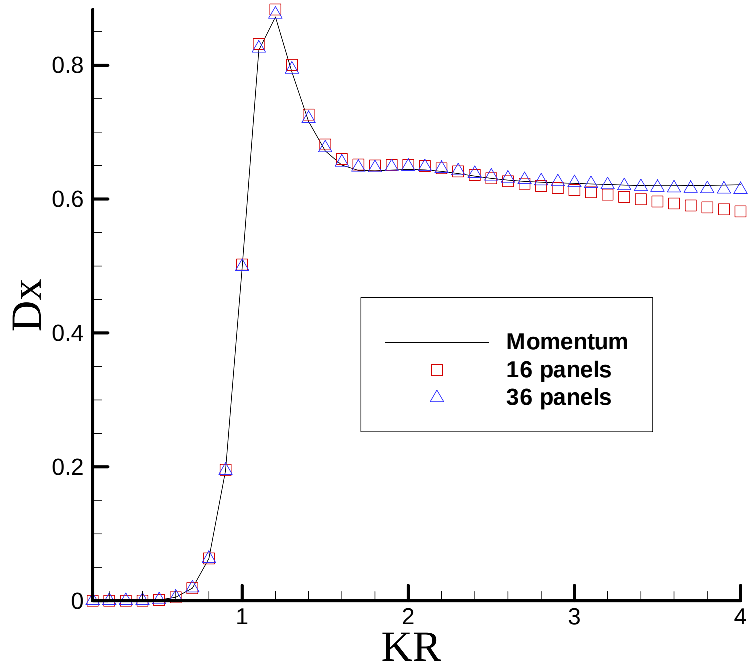

Example 2 – barge created by MultiSurf (test20)

Barge
length 100m, beam 20m, draft 4.8m

Control Surface (Box without free surface. Good for horizontal forces and yaw moment by Alternative 1)
lengh 120m, beam 30m, draft 10m

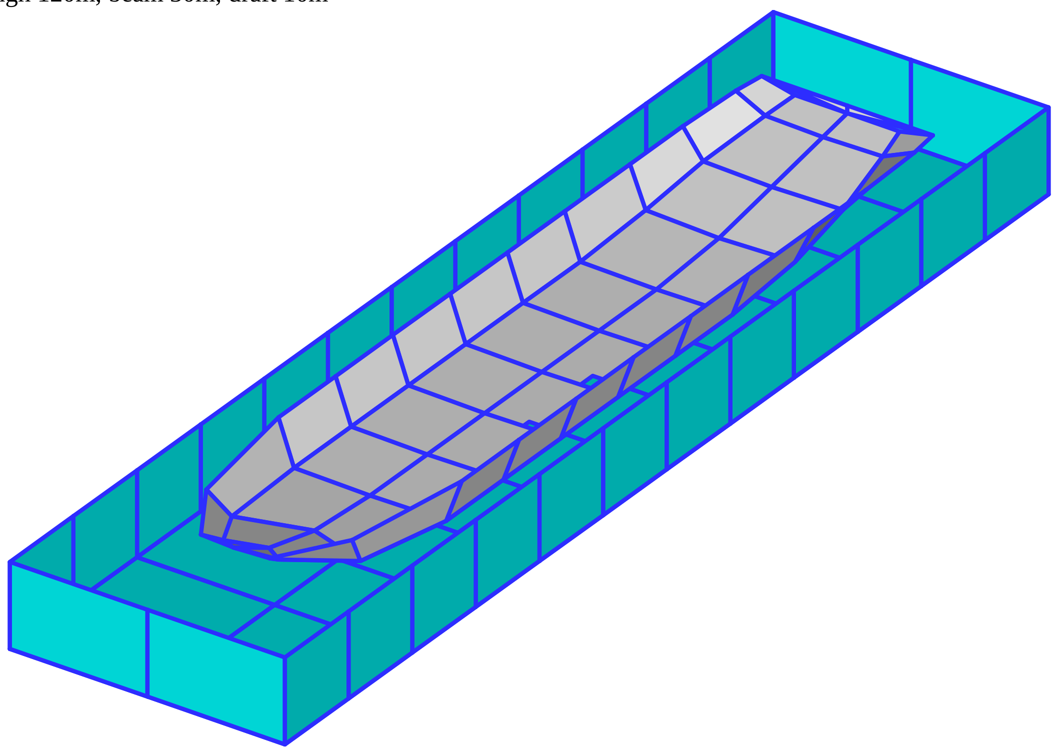

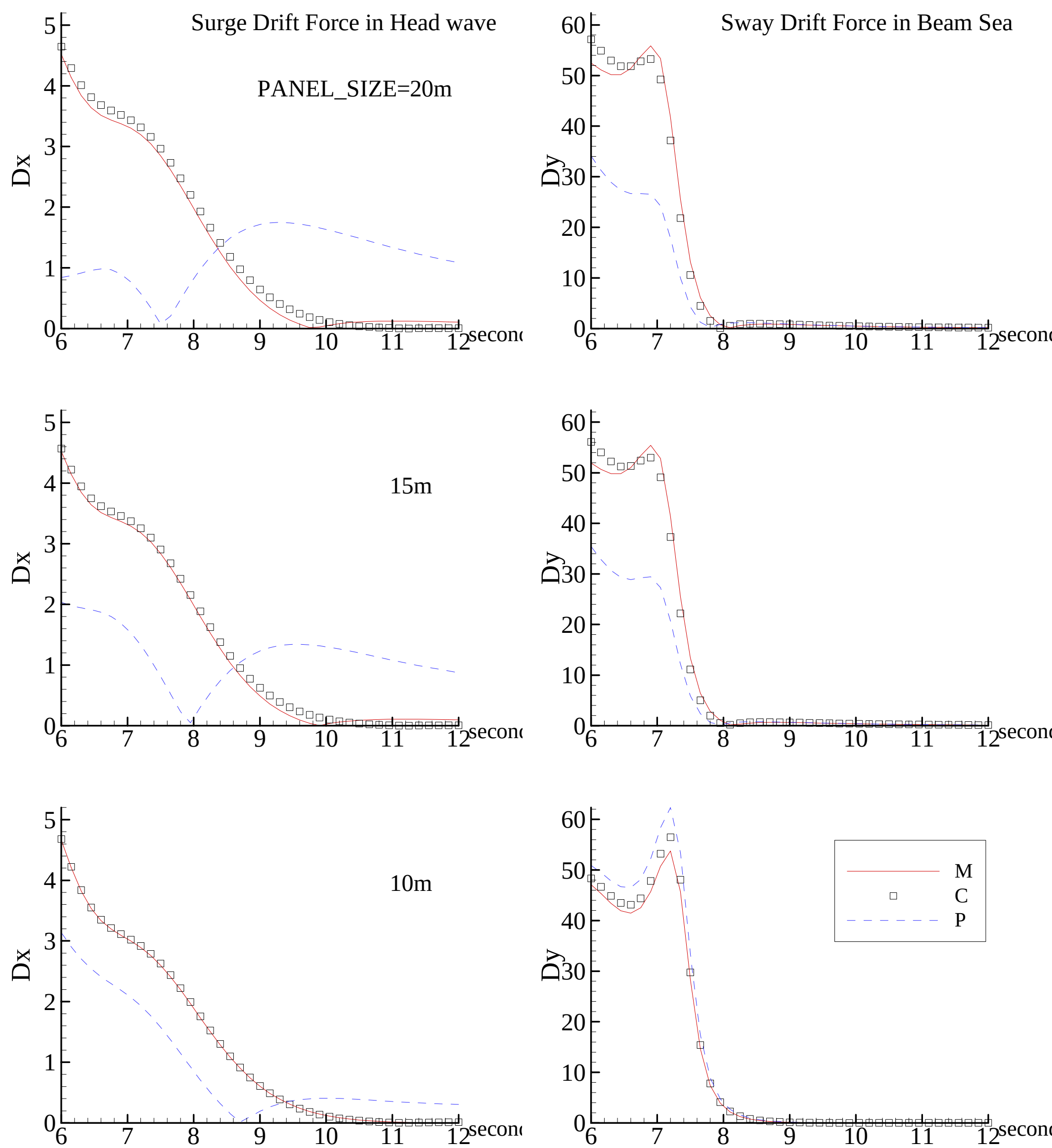

Surge Drift Force in Head wave
PANEL_SIZE=20m
Sway Drift Force in Beam Sea
15m
10m
Dx
Dy
second
M
C
P

Example 3 – body with non-vertical wall

Skewed hemisphere with radius 1 on the free surface
Control surface: radius and draft 1.2
Mesh is the higher-order panels
4th order Gauss quadrature on the control surface

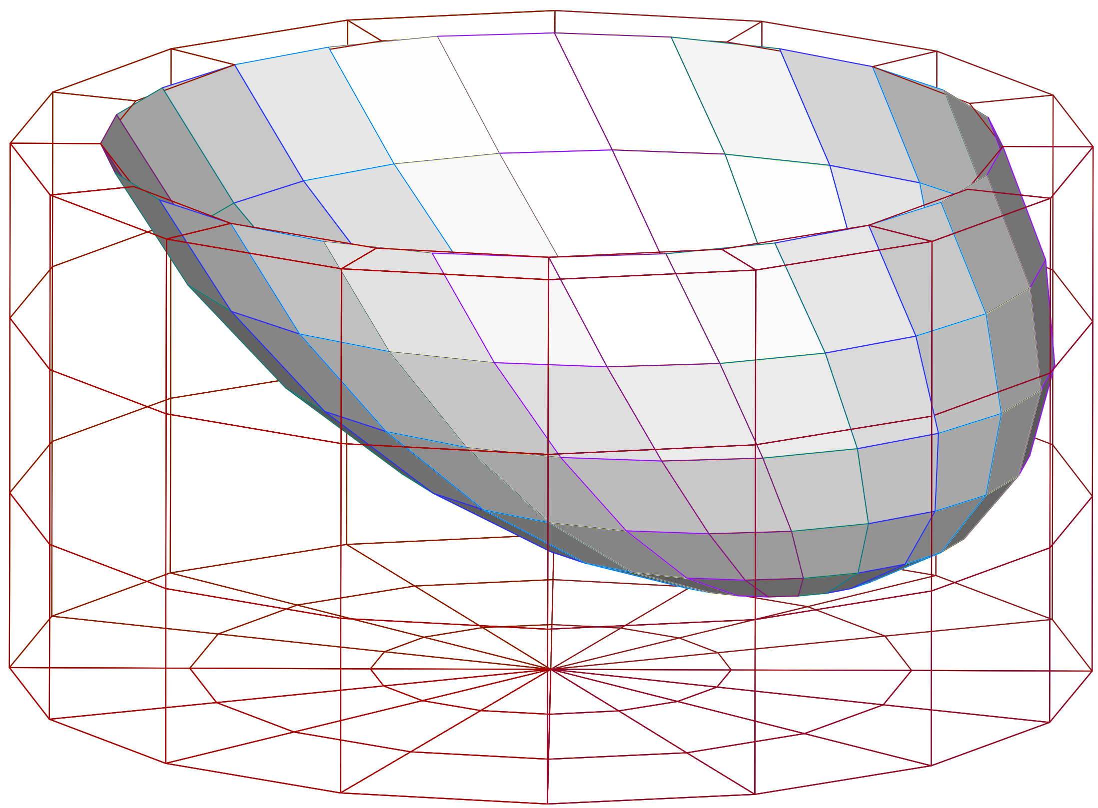

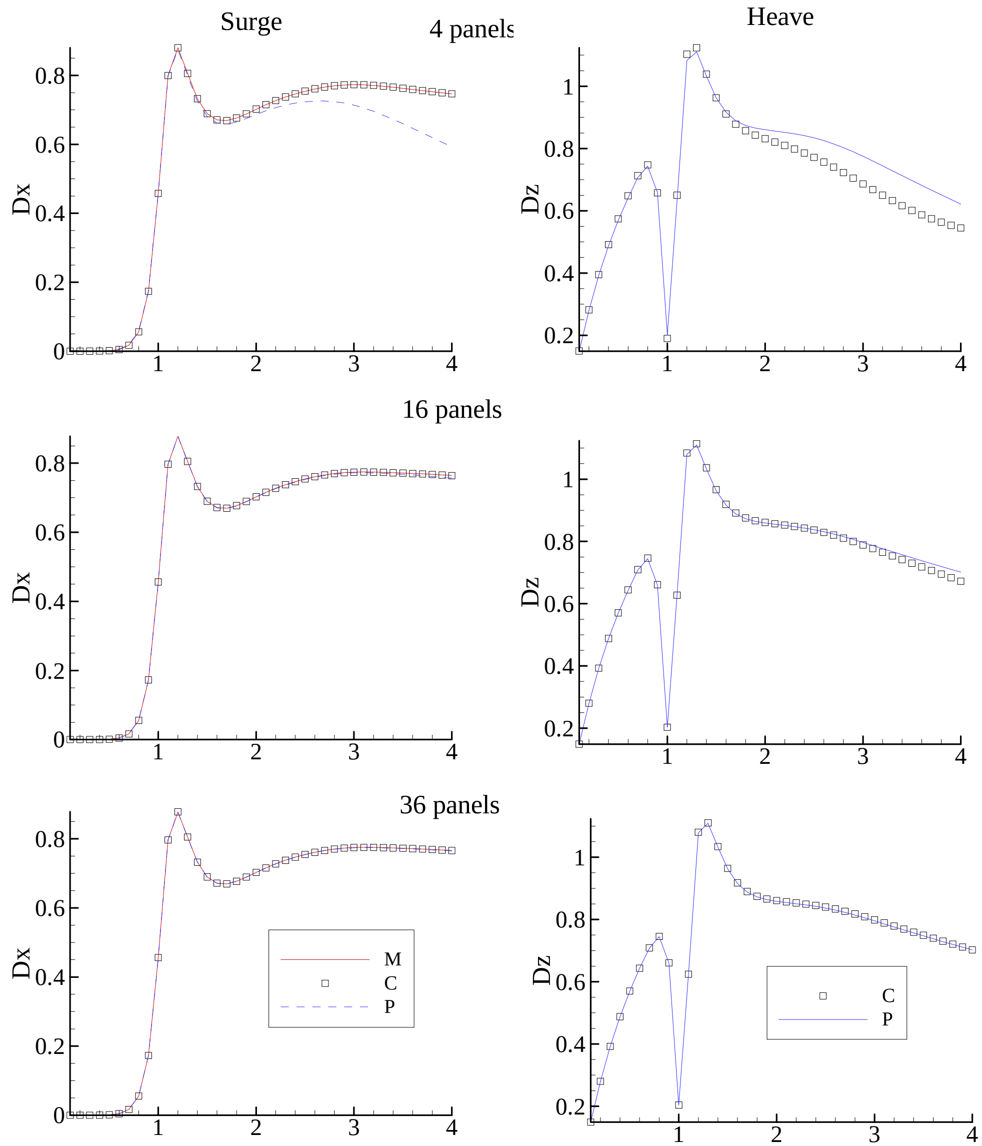
Surge
4 panels
Heave
16 panels
36 panels
Dx
Dz
M
C
P
C
P

7. Example 4 – body with dipole element

When ILOWHI=1, control surface option can be applied for bodies with dipole elements when they are submerged or intersect the free surface perpendicularly (exceptions are surge and sway forces and yaw moment when evaluated by Alternative 1. They are not subject to this restriction).

Example shown here is the spar with strakes in Test 21.

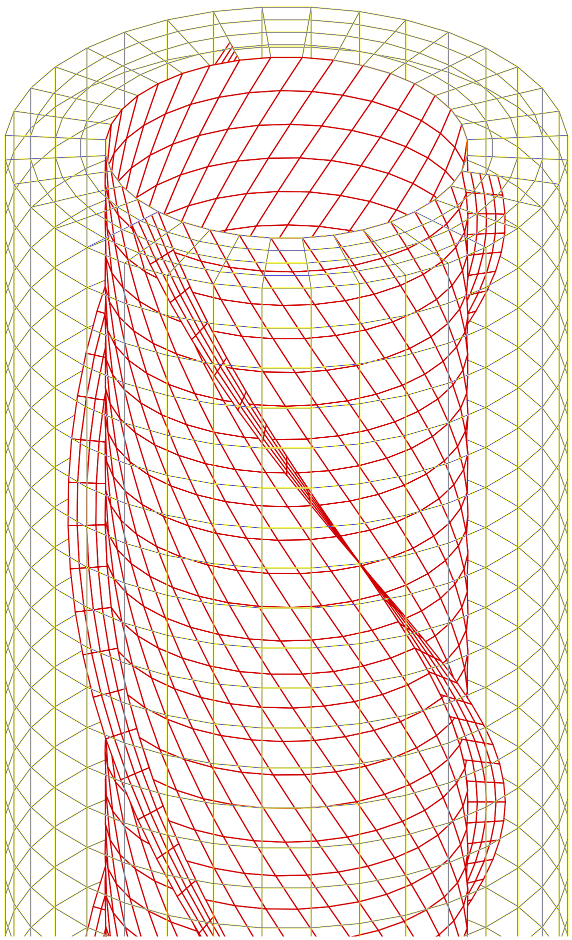

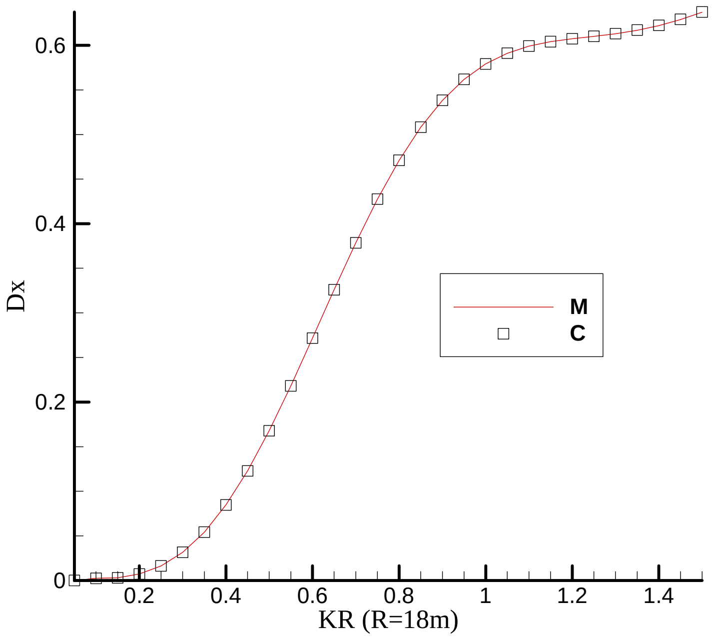
Dx
0.6
0.4
0.2
0
0.2
0.4
0.6
0.8
1
1.2
1.4
KR (R=18m)
M
C

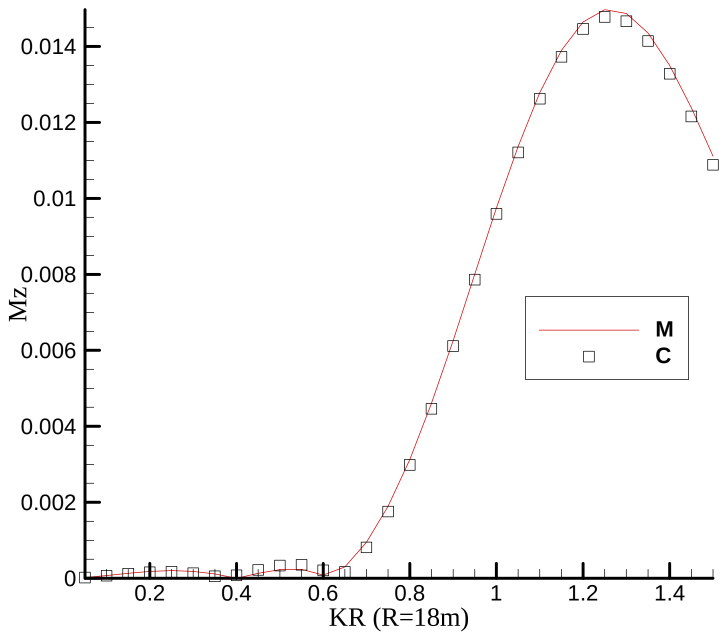
Mz
0.014
0.012
0.01
0.008
0.006
0.004
0.002
0
0.2
0.4
0.6
0.8
1
1.2
1.4
KR (R=18m)
M
C

Summary

A) Control surface method was implemented to provide an optional method when the traditional momentum or pressure mean forces are not available or not robustly evaluated as shown in the examples

B) The control surface mean force is as accurate as the momentum mean force for practical purpose.

C) The run time of FORCE module is same order as POTEN module and could be longer. But overall computational time can be reduced because POTEN run does not require fine discretization as was the case for pressure mean forces.

D) CSF must be prepared. All available GDF can be easily converted into CSF but the free surface part of the control surface have to be included for vertical momentum. For horizontal momentum, a few generic geometry such as rectangular box should be sufficient.

E) The effect of the tank is added in the same manner as the conventional pressure mean forces, by integrating the quadratic pressure inside the tank surface.

Radiated Wave Field From a Bank of Wavemakers (Test23)

By J. N. Newman

V6.3 includes a new option, motivated by John O'Dea for a project to design new wavemakers for the basin at Carderock. The proposed wavemakers are rectangular flaps, located in the planes of two adjacent tank walls (at right angles). The number of individual wavemakers is large. The principal interest is to predict the radiated wavefield at a large number of field points.

8 wavemakers in the wall x=0

Wavemaker width/depth = 1m by 2m

Wavemakers are hinged about z=-2m

Water depth = 4m

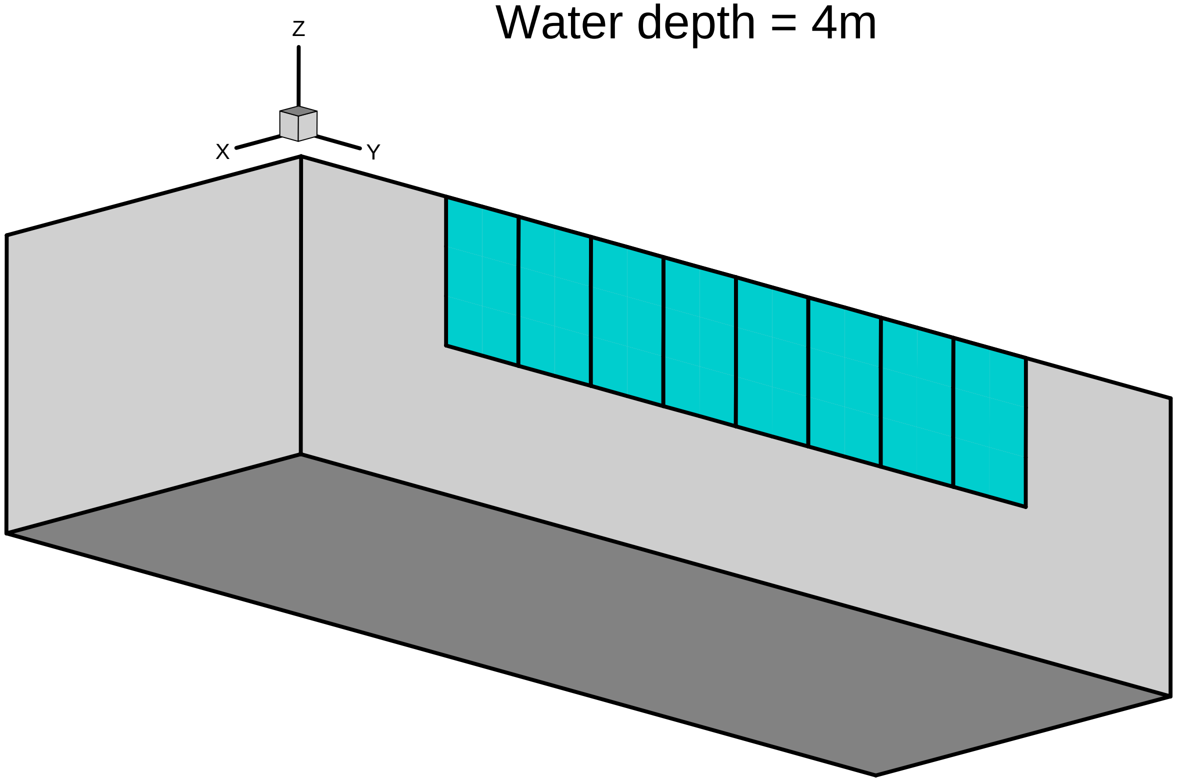

The `conventional’ approach using WAMIT would require that a small thickness be added to each wavemaker, thus it would protrude from the wall. From theory we know there is a simpler solution, with sources of known strength (proportional to the normal velocity) in the plane of the wavemaker.

Computational Approach

- Represent geometry by low- or higher-order panels/patches (wet side only)
- Set up RHS of linear system (source strength)
- Set velocity potential = 0 on body surface, and skip solution of linear system (ISOLVE=-1)
- Only radiation modes are considered, no incident waves or diffraction.
- Supported outputs include only options 6&7 (wave elevations, pressures, fluid velocities)
- No other bodies can be present in the fluid domain
- Other walls are open boundaries

- For details see User Manual Section 10.8 and Test23
- New option for rectangular arrays of field points (Section 3.10) simplifies input data for large numbers of field points

Evaluation of quadratic forces in bi-chromatic waves using control surfaces

The total force on the body

$$\vec{F} = -\rho \iint_{s_b} \vec{n}[\Phi_t + \frac{1}{2}\nabla\Phi \cdot \nabla\Phi + gz]ds$$

can be expressed in terms of the momentum flux over s_c, s_f, hydrostatic

forces on s_b and $-d\bar{\mathbf{P}}/dt$, negative rate of change of the momentum in the volume inside s_{bfc}

$$\begin{aligned}\vec{F} &= \rho \iint_{s_c} [(\Phi_t + \frac{1}{2}\nabla\Phi \cdot \nabla\Phi)\vec{n} - \frac{\partial \Phi}{\partial n}\nabla\Phi]ds \\ &+ \rho \iint_{s_f} (\Phi_t + \frac{1}{2}\nabla\Phi \cdot \nabla\Phi)\vec{n}ds - \rho g \iint_{s_b} z\vec{n}ds - \frac{d\mathbf{P}}{dt}\end{aligned}$$

For monochromatic waves, the time average of $\dfrac{d\bar{\mathbf{P}}}{dt} = 0$ and the mean forces are obtained from the quadratic terms of the momentum flux.

For bichromatic waves, the change of momentum in the volume should be added. Expressed in terms of momentum flux on s_{bfc}, it takes a form

$$\frac{d\mathbf{P}(t)}{dt} = \rho \frac{d}{dt} \iiint \vec{V} dv = \rho \iint_{s_{bfc}} [\Phi_t \vec{n} + \nabla \Phi (\vec{U} \cdot \vec{n})] ds$$

The quadratic components about the mean surface takes a form

$$\begin{aligned} \frac{d\mathbf{P}^{(\mathbf{2})}(t)}{dt} &= \rho \iint_{S_b} \phi_t (\vec{\alpha} \times \vec{n}) + (\vec{\Xi} \cdot \nabla \phi_t) \vec{n} + \nabla \phi (\vec{\Xi}_t \cdot \vec{n}) ds + \rho \int_W (\zeta - \Xi_3) \phi_t \vec{n}' dl \\ &+ \rho \iint_{S_f} \nabla \phi \frac{\partial \phi}{\partial n} + \zeta \frac{\partial \phi_t}{\partial z} \vec{k} - \zeta \nabla' \phi_t ds + \rho \int_W \phi_t (\vec{\Xi} \cdot \vec{n}') dl \\ &+ \rho \int_C \zeta \phi_t \vec{n}' dl \end{aligned}$$

Using the relations

$$\frac{1}{2}\rho\int_{W+C}\vec{n}'\zeta\phi_t dl = \rho\iint_{S_f}\zeta\nabla'\phi_t ds$$

and

$$\int_W \phi_t[(\vec{\Xi}\cdot\vec{n}')\vec{k} - \Xi_3\vec{n}']dl + \iint_{S_b}\phi_t(\vec{\alpha}\times\vec{n})ds = \iint_{S_b}[(\vec{\Xi}\cdot\vec{n})\nabla\phi_t \ - \ \vec{n}(\vec{\Xi}\cdot\nabla\phi_t)]ds$$

the rate of momentum change can be simplified in the form

$$\frac{d\mathbf{P}^{(2)}(t)}{dt} \ = \ \rho\iint_{S_f}[\nabla\phi\frac{\partial\phi}{\partial n} + \zeta\nabla\phi_t]ds + \rho\iint_{S_b}[\nabla\phi(\frac{d\vec{\Xi}}{dt}\cdot\vec{n}) + (\Xi\cdot\vec{n})\nabla\phi_t]ds$$

The quadratic force in bichromatic waves is then obtained from

$$
\begin{aligned}
\vec{F}^{(2)} = \; & - \; \frac{1}{2}\frac{\rho}{g}\int_C \vec{n}'\phi_t^2 dl - \rho g \int_W [\zeta(\vec{\Xi}\cdot\vec{n}')]\vec{k}dl \\
& - \; \rho \iint_{S_c} [\nabla\phi \frac{\partial \phi}{\partial n} - \frac{1}{2}\vec{n}(\nabla\phi\cdot\nabla\phi)]ds \\
& + \; \rho\vec{k} \iint_{S_f} (\zeta \frac{\partial \phi_t}{\partial z} + \frac{1}{2}\nabla\phi\cdot\nabla\phi)ds + \vec{F}_S^{(2)} \\
& - \; \rho \iint_{S_f} [\nabla\phi\frac{\partial\phi}{\partial n} + \zeta\nabla\phi_t]ds - \rho \iint_{S_b} [\nabla\phi(\frac{d\vec{\Xi}}{dt}\cdot\vec{n}) + (\Xi\cdot\vec{n})\nabla\phi_t]ds
\end{aligned}
$$

Sphere sum frequency (KR1=KR KR2=KR+0.4)

P: Pressure integration
C: Control Surface

1: 1 x 1 panels
2: 2 x 2
3: 4 x 4

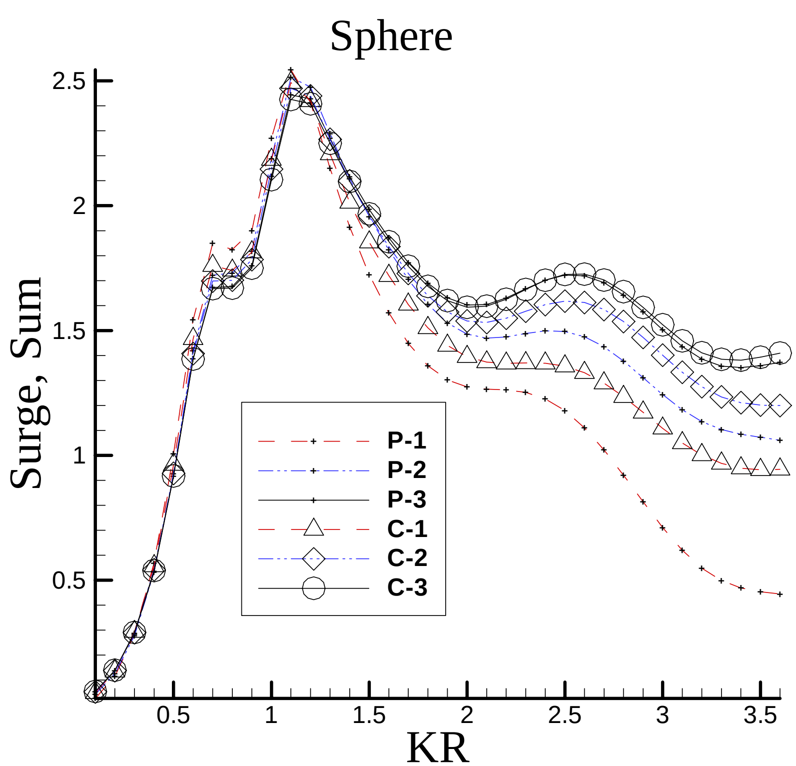

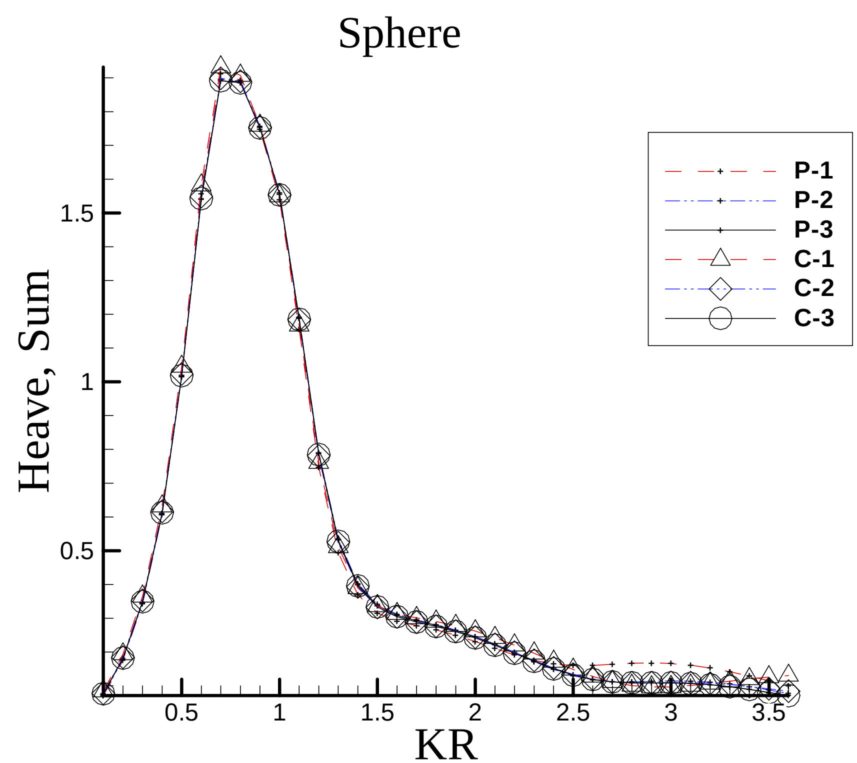

Sphere difference frequency (KR=KR-0.4, KR2=KR)

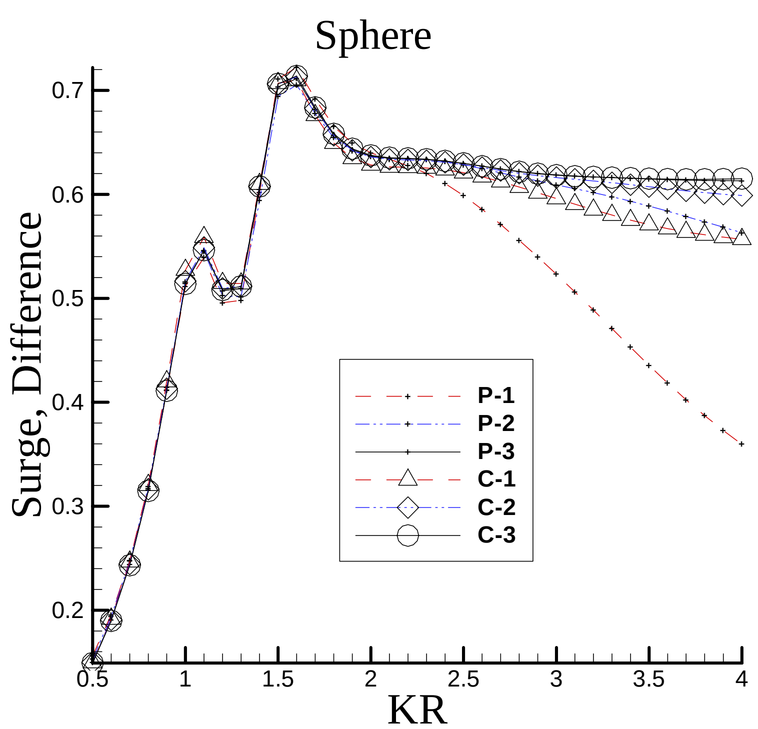

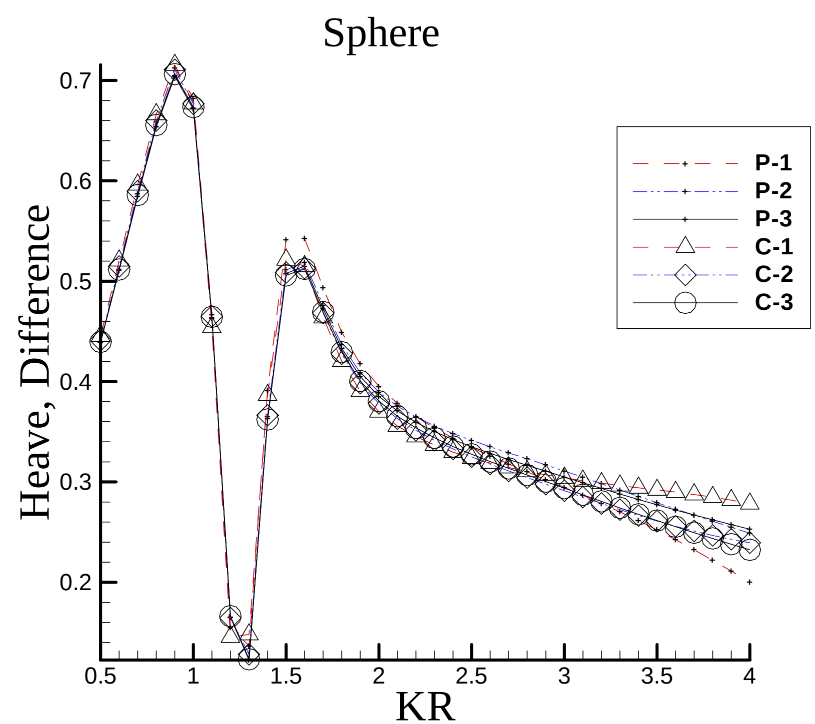

Cylinder sum frequency R=1, D=1 (KR1=KR KR2=KR+0.4)

P: Pressure integration
C: Control Surface

1: 1 x 1 panels (side and bottom)
2: 2 x 2
3: 4 x 4

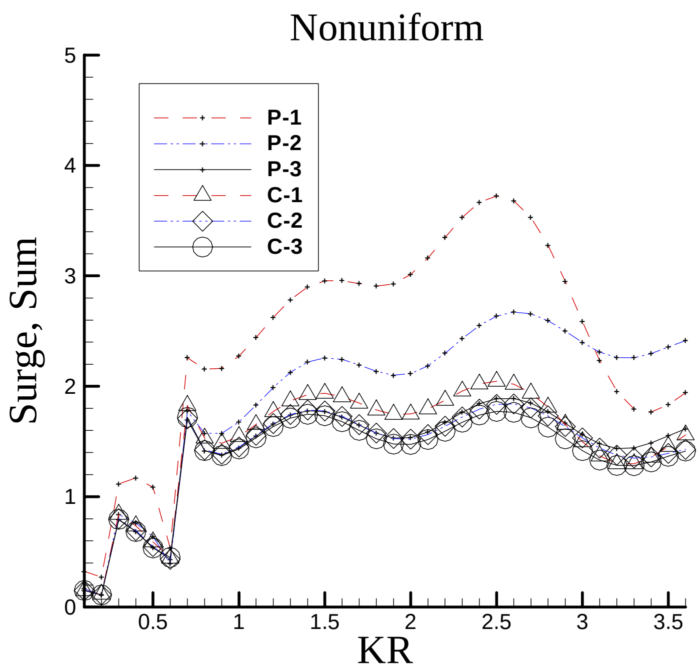

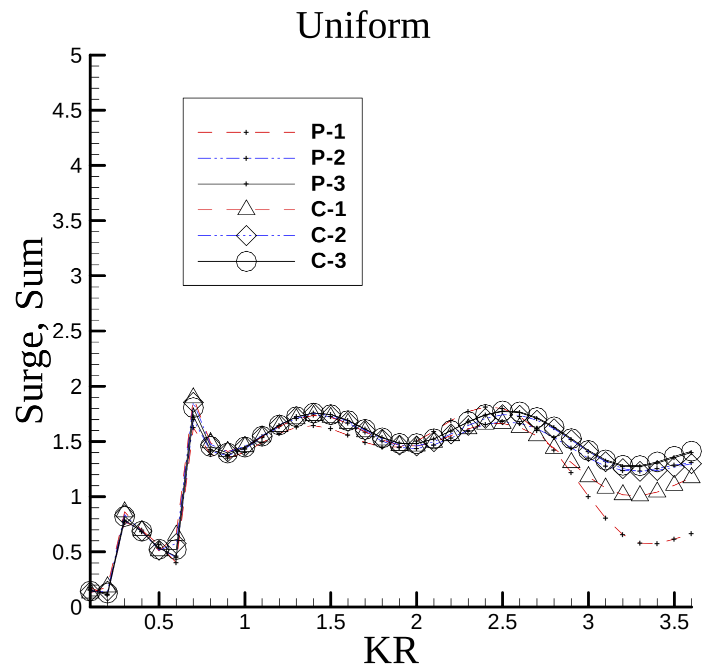

Cylinder diff frequency R=1, D=1 (KR1=KR-0.4 KR2=KR)

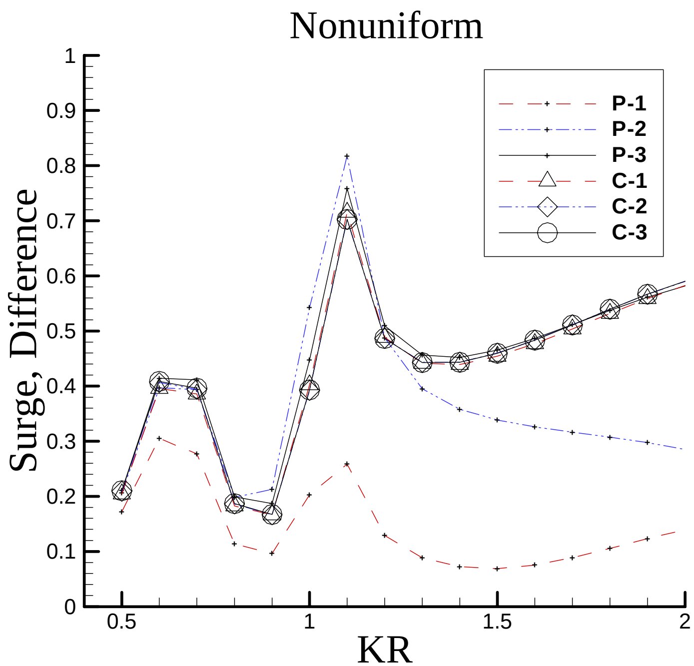

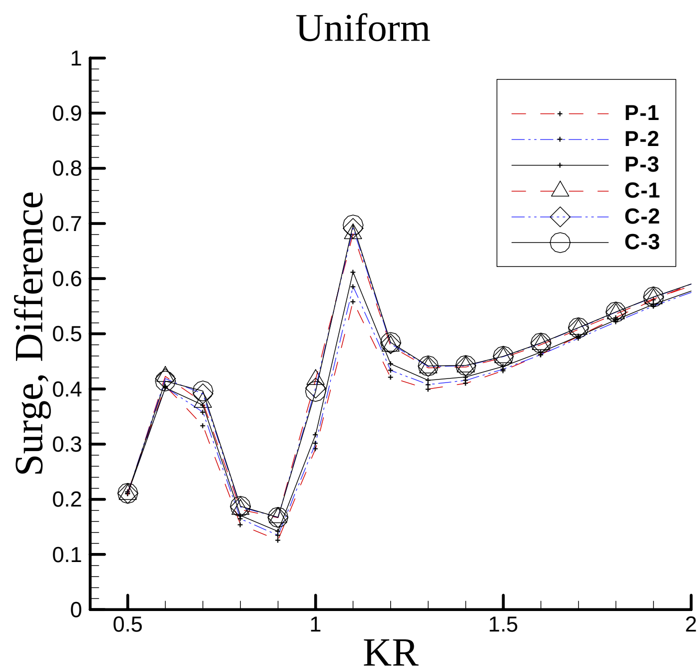

Cylinder sum frequency R=1, D=1 (KR1=KR KR2=KR+0.4)

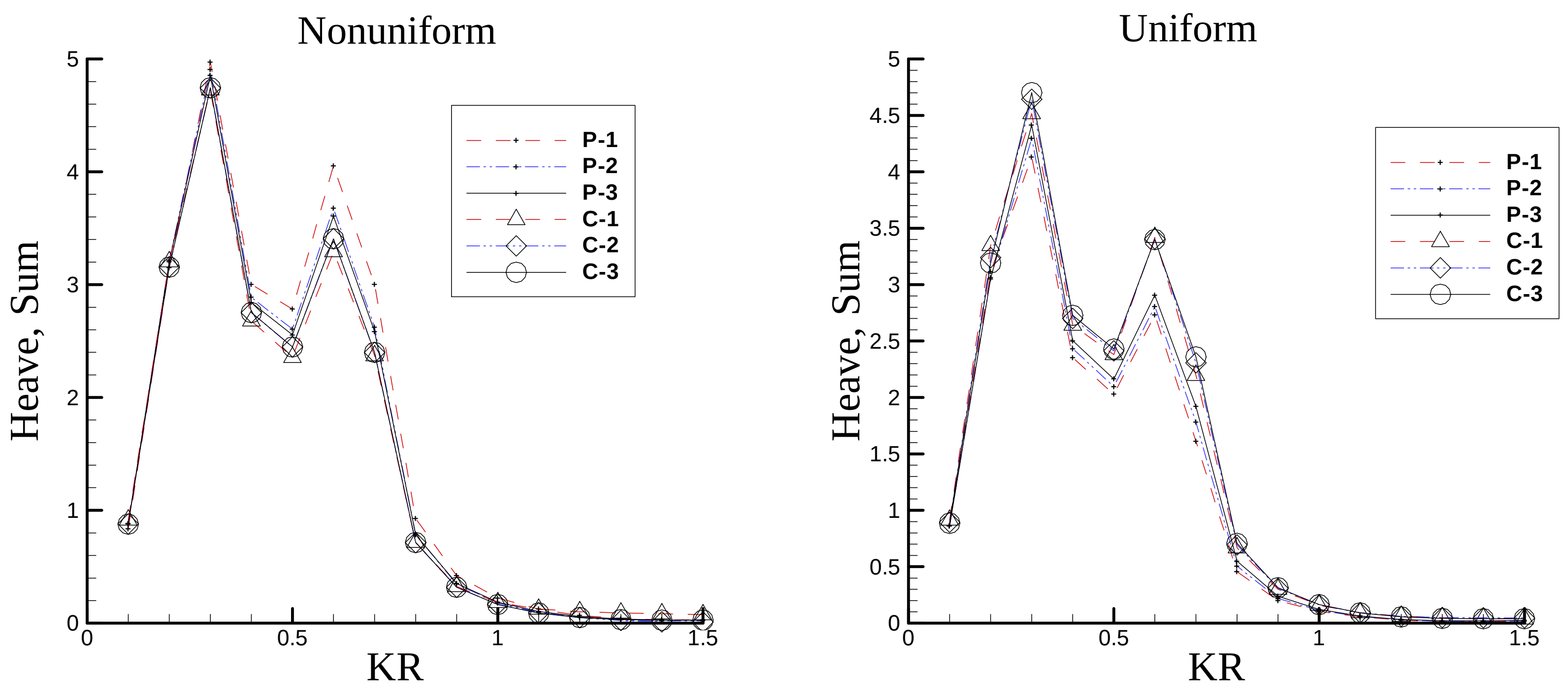

Cylinder diff frequency R=1, D=1 (KR1=KR-0.4 KR2=KR)

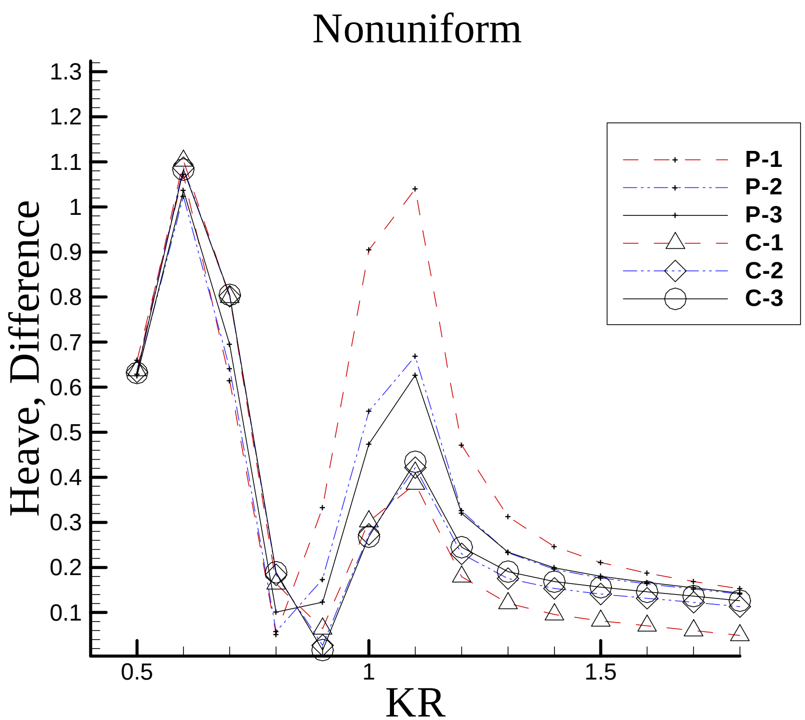

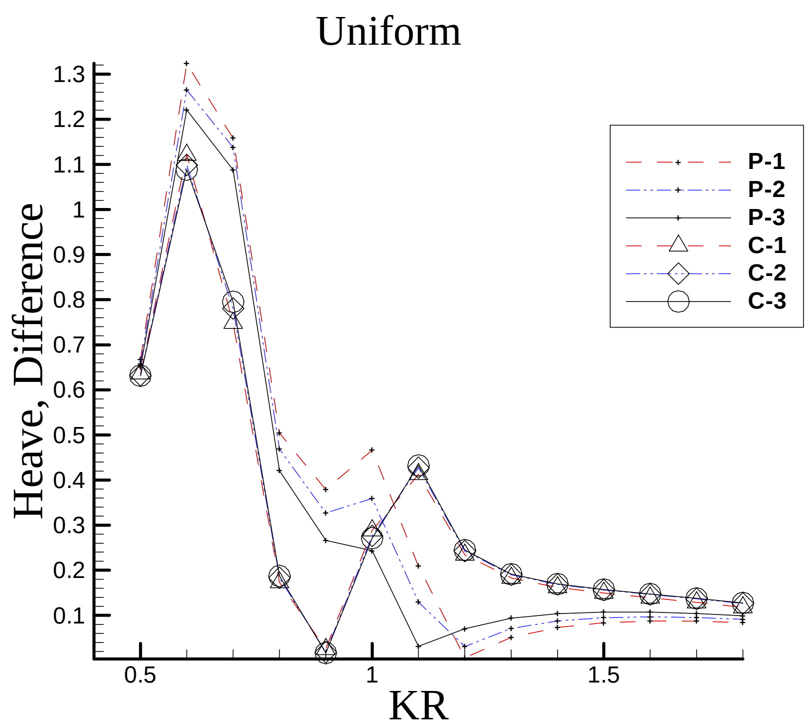

Summary

1. An expression for quadratic forces in terms of the momentum flux on Control Surface is derived. Unlike the mean drift forces, the expression also includes the quadratic pressure on the body which is linearly proportional to the fluid velocity.

2. The computational results for a sphere and a truncated cylinder indicate the expression calculates the forces more efficiently and consistently than conventional pressure integral.

3. Unlike the mean forces, the free surface should be included in CSF even for the horizontal forces and yaw moment

Progress for WAMIT V6.3S

Extensions were made for the evaluation of quadratic forces.

a) Internal tanks
b) Flexible lids on the free surface
c) Control surface option

Current work on V6.3S

a) internal tanks for complete 2^{nd}-order solution
b) B-spline fitting of the pressure and velocity on the free surface for efficient evaluation of the free surface forcing in the higher-order method

Illustrative example - quadratic force on a vessel with 4 tanks

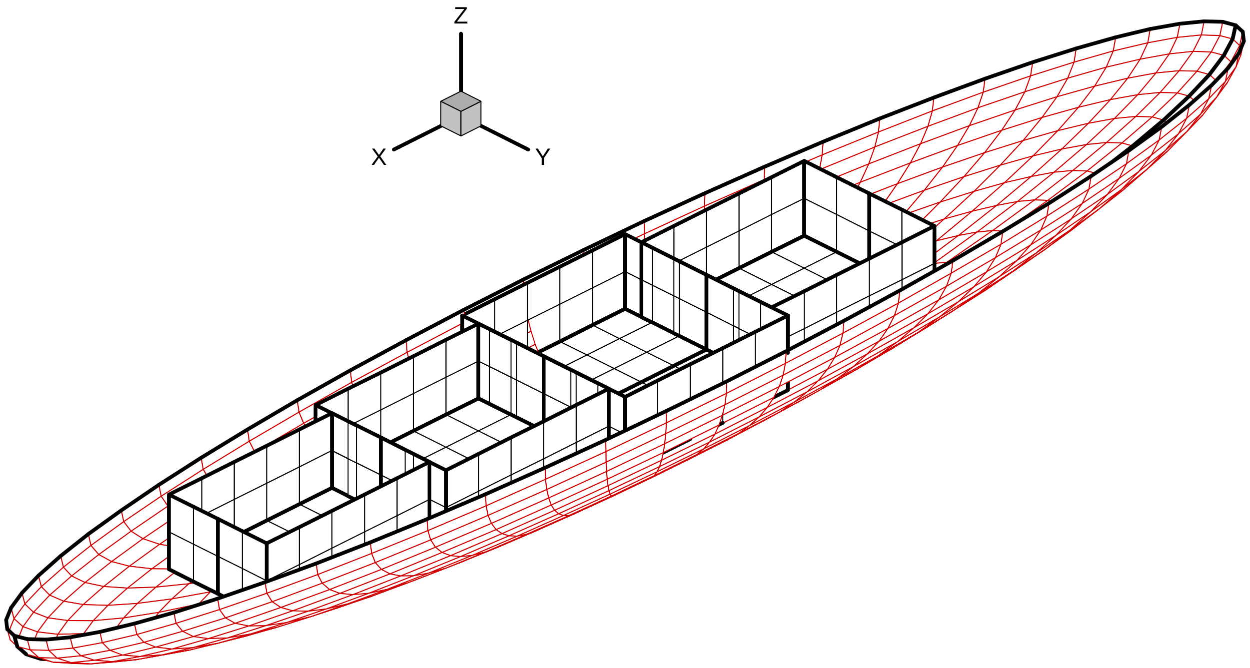

Sway force in beam sea

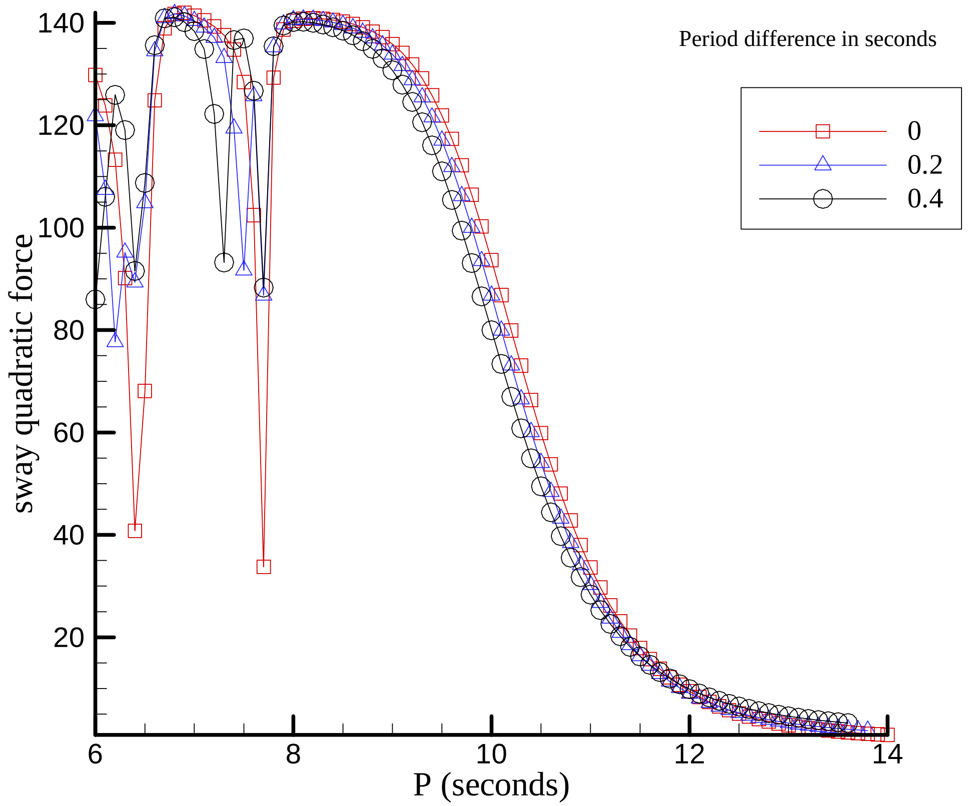

Sway force QTF matrix in a beam sea

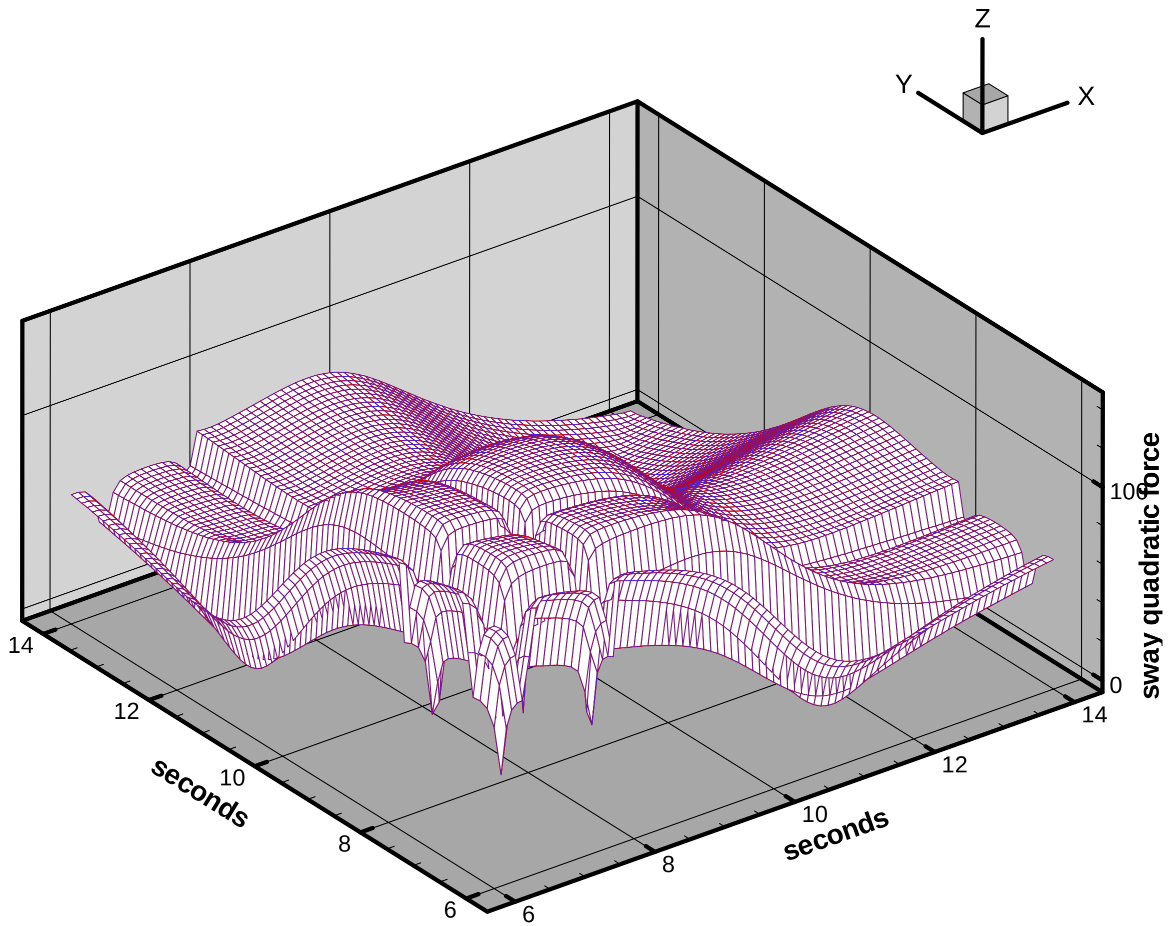

Using WAMIT with trimmed waterlines

By J. N. Newman

Background

During a visit with John Letcher he indicated the interest of Petrobras and São Paulo in running WAMIT with different waterlines (floatation planes), without the need to re-discretize the body for each waterline. (Work on this started after the release of V6.3.)

General Approach

- Body geometry must be defined up to at least the plane of the free surface, and may extend above this plane
- Geometry, and hydrodynamic outputs, are defined relative to conventional body-fixed coordinates
- New parameter ITRIMWL=0 (default) or 1 in config file
- New array XTRIM in config file, specifying the vertical displacement (heave) and trim (pitch, roll) relative to the origin of the body coordinates. (Pitch, roll are Euler angles, in that order.)
- WAMIT trims the waterline, including only the portion of the geometry below Z=0 (global plane of free surface)
- Details are different for low-order panels and higher-order patches

Low-order Approach (ILOWHI=0)

- First check all panels, eliminate `dry panels' and modify waterline panels which span Z=0:
- Case 1: waterline intersects two opposite sides of a quadrilateral panel – simply lower the top vertices down to the waterline
- Case 2: waterline intersects two adjacent sides with a triangular submerged portion – same approach, with a triangular wet panel
- Case 3: waterline intersects two adjacent sides with a 5-sided submerged portion: this must be subdivided into two new panels
- NEQN is reduced for dry panels, increased for Case 3

TEST07
(draft=35m)

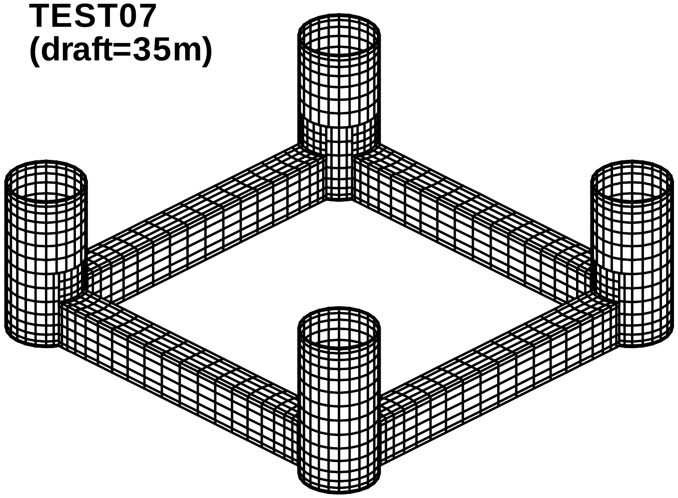

XTRIM= 17.5, 10, 10

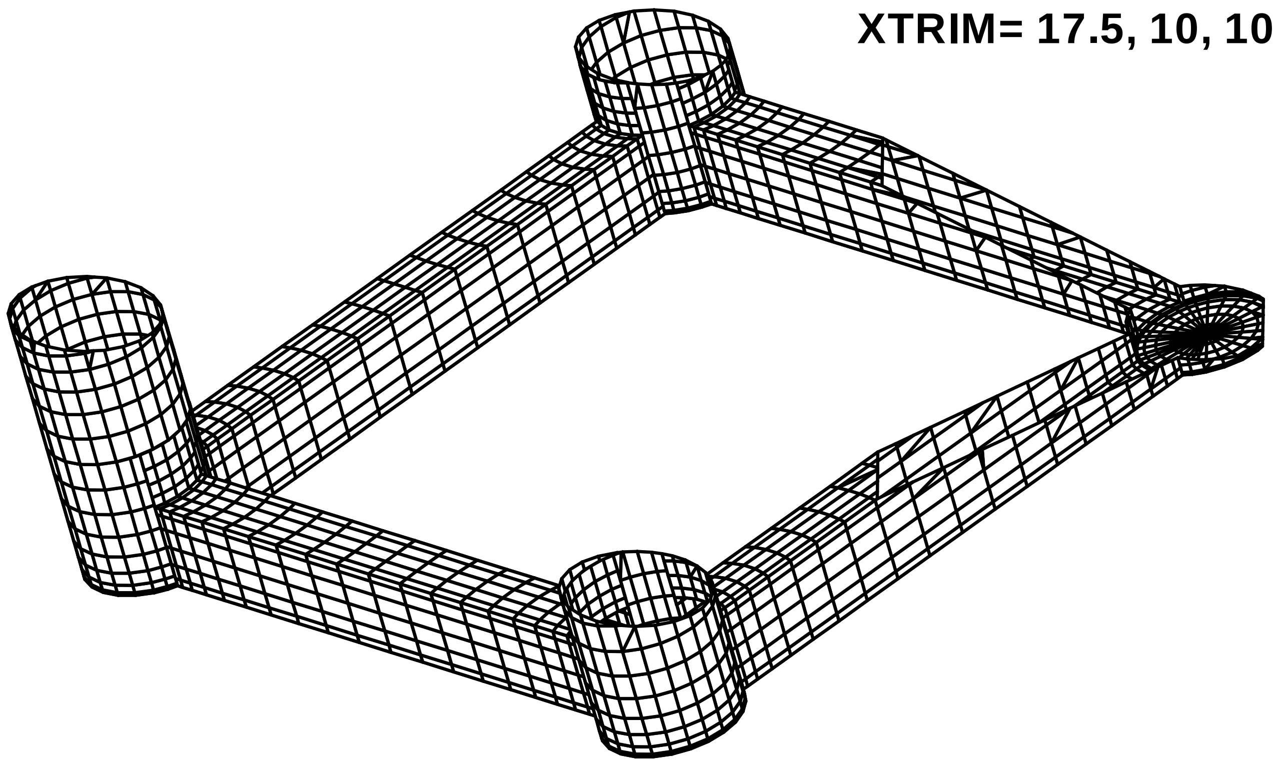

TEST09.GDF
(draft=200m)

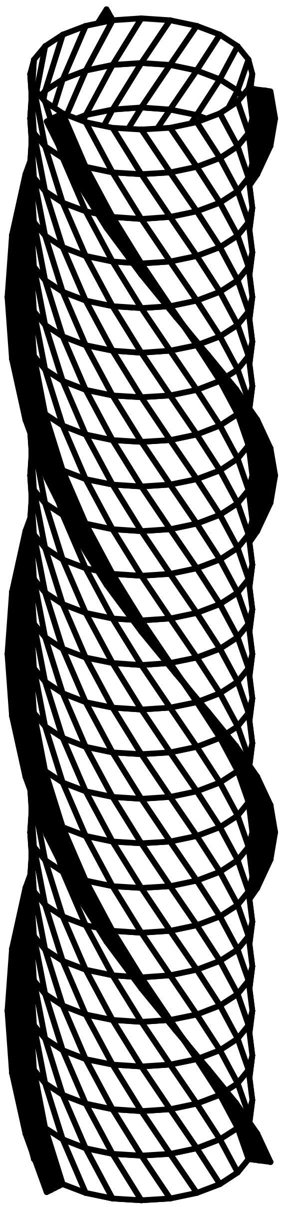

XTRIM=150 30 0

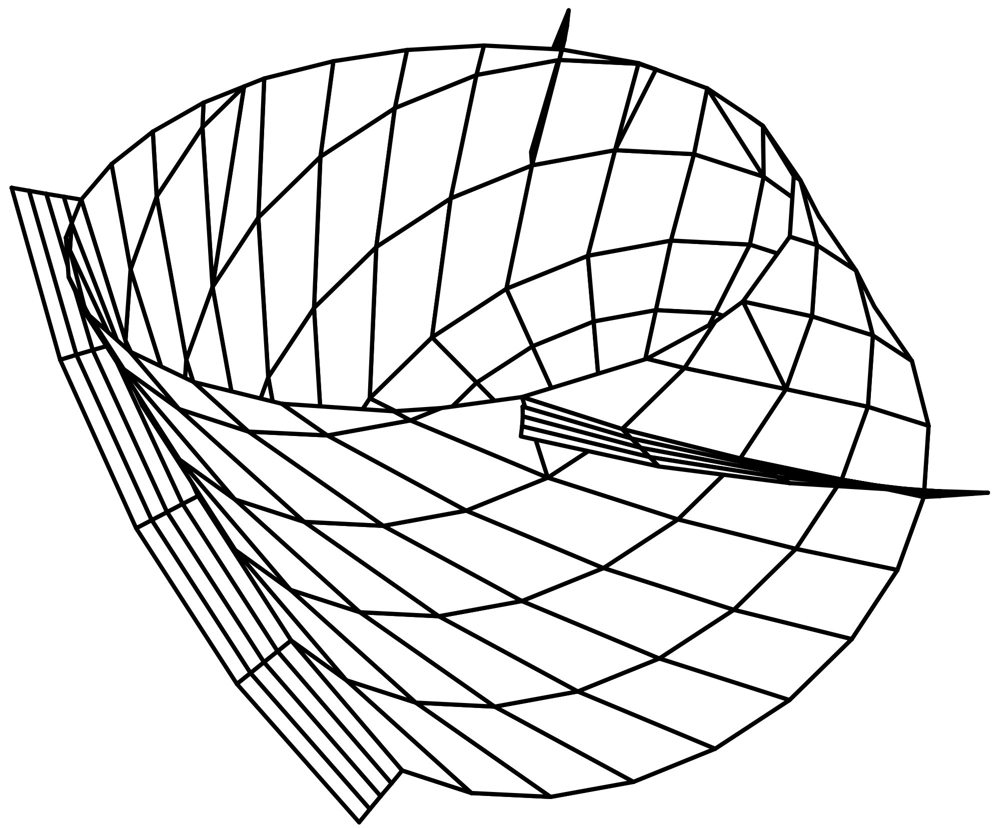

TEST05

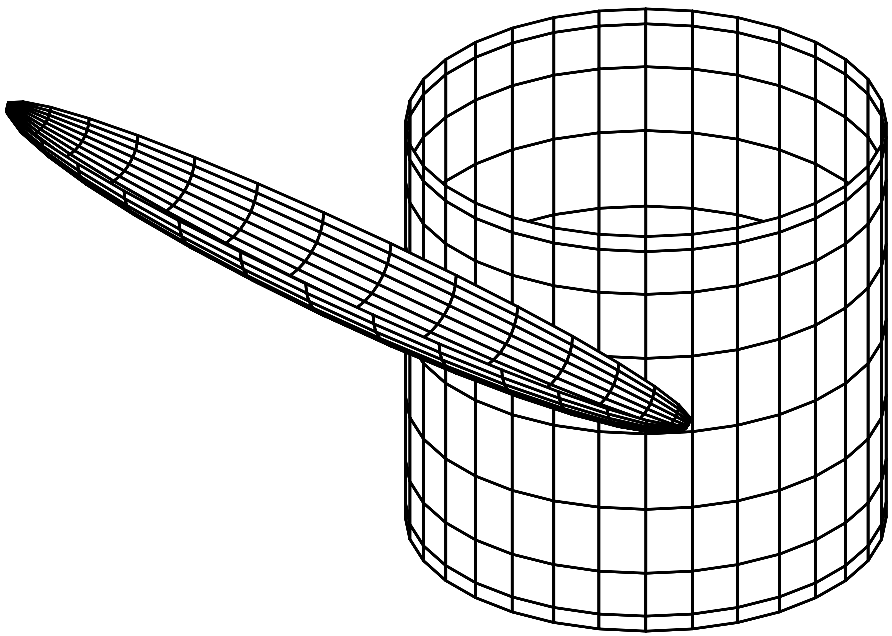

XTRIM(1)= 1.0 10 0

XTRIM(2)= 0.1   0 0

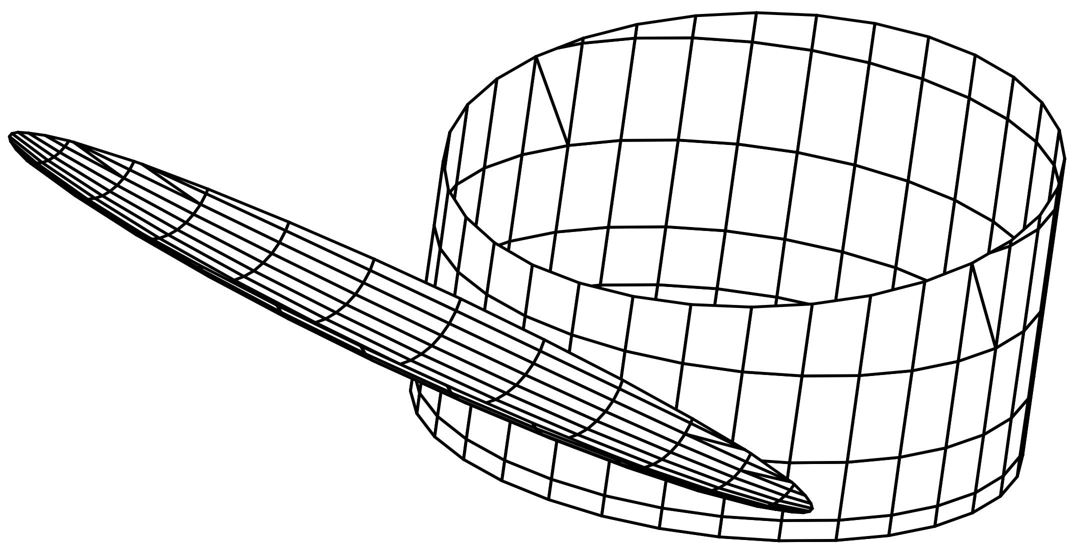

Higher-order Approach (ILOWHI=1)

- First check all patches, eliminate if `dry’ and tag waterline patches which span Z=0
- For waterline patches the computational domain (parametric) (U,V)=(-1,1) is mapped to the submerged portion of the patch
- If submerged portion is `triangular’, a singular point is introduced at the submerged vertex
- If submerged portion is `5-sided’ a weak singular point is introduced at the knuckle between the waterline and patch side
- NPATCH is reduced for dry panels

XTRIM(1)= 0 0 0

XTRIM(2)= 0 0 0

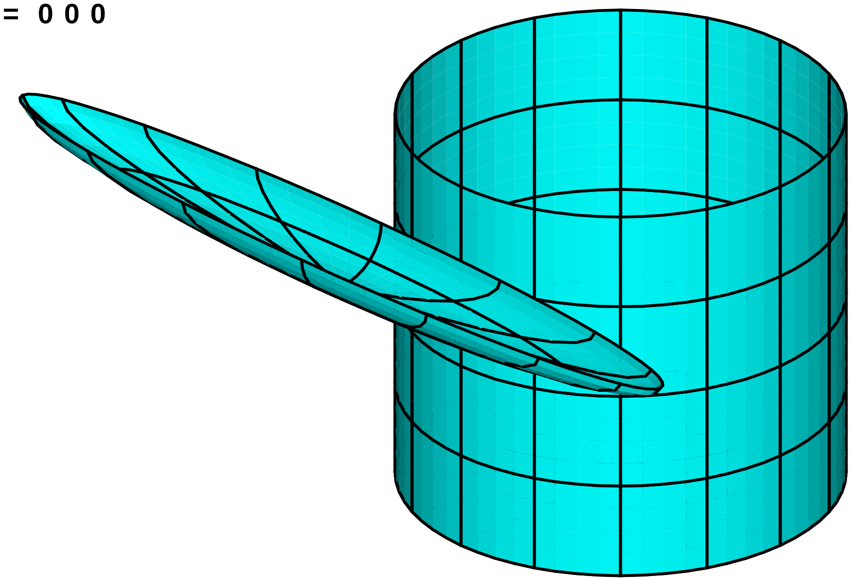

XTRIM(1)= 1.0 10 0

XTRIM(2)= 0.1   0 0

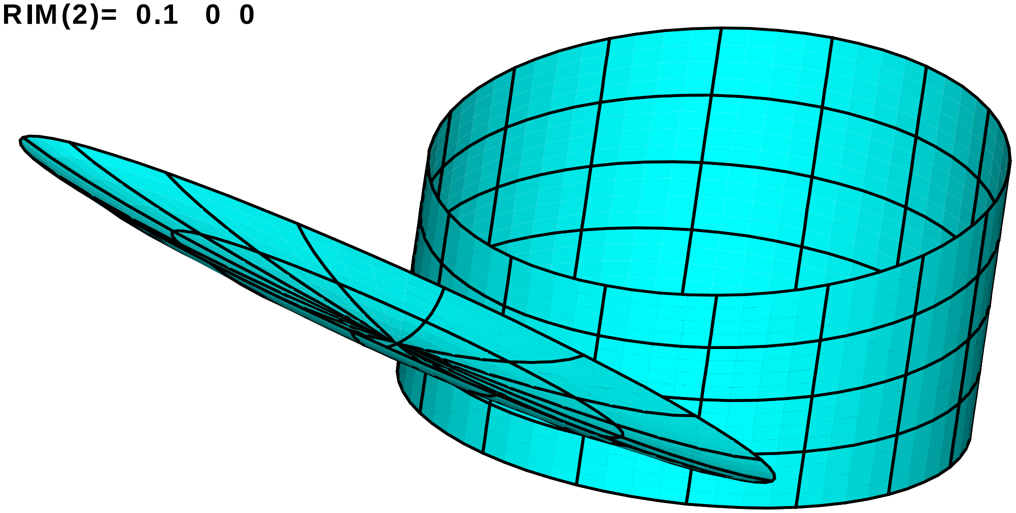

XTRIM = 0.5 0 0

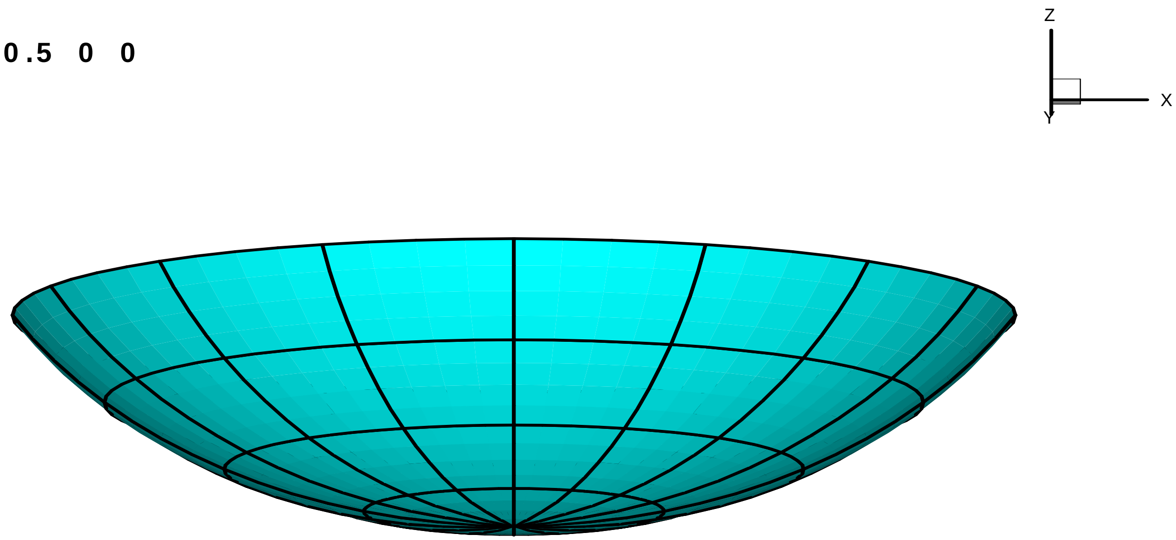

XTRIM = 0.5 25 0

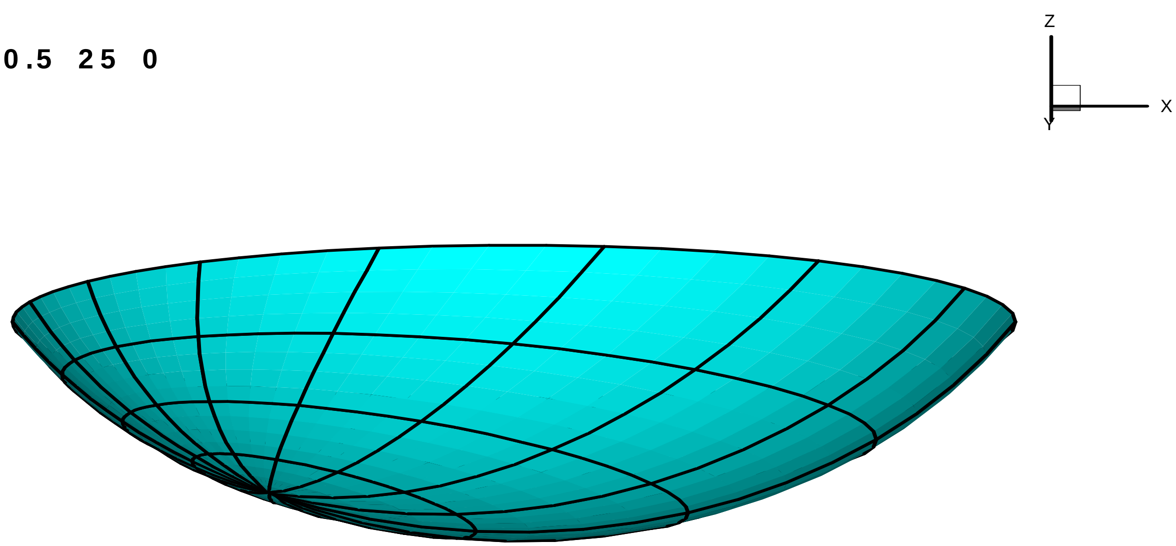

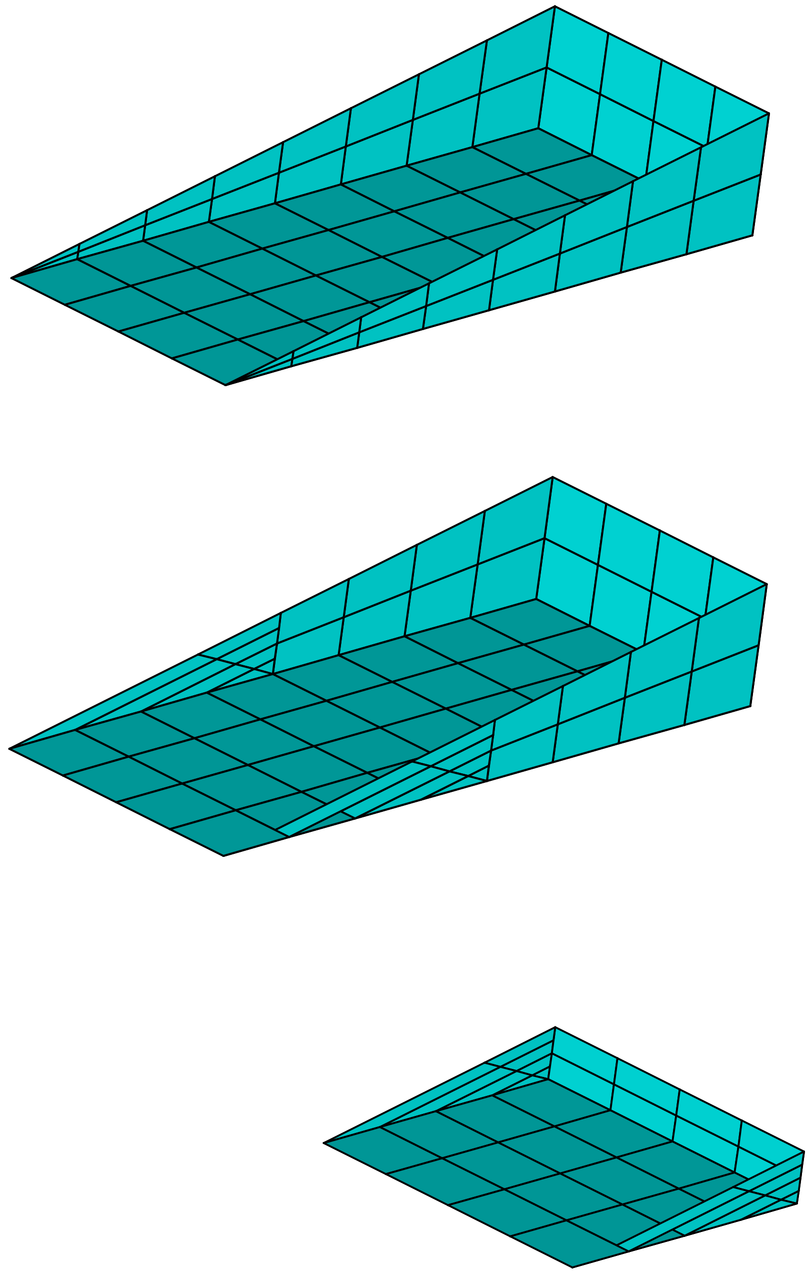

Special Points

- If ITRIMWL=1 the error message regarding panel/patch vertices above the free surface is disabled
- IRR=1 requires user to represent interior free surface (awkward)
- IRR=2 (projection of panels onto free surface) may be affected by pitch and roll displacements
- Angular displacements may affect symmetry. WAMIT automatically reflects when this is necessary, as in the TLP example.
- Internal tank waterlines are not trimmed. Special attention is required for tank free surface if angular displacements are included.
- Trimming of higher-order patches could fail if the trace of the waterline is irregular in parametric space

Status

- Low-order has been tested with good results
- Higher-order still being debugged
- Expect to include in V6.4
- Beta version can be released to Consortium Members on request

Current Participants

ChevronTexaco

ConocoPhillips

Norsk Hydro

OTRC

Petrobras/USP

Shell

Statoil

Marcos Ferreira
Petrobras
CENPES/PDP/MC
Cidade Universitaria Quadra 7
21949-598 Ilha do Fundao
Rio de Janeiro, Brazil
marcos.donato@petrobras.com.br

Tim Finnigan
Chevron Energy Technology Co.
6001 Bollinger Canyon Road
Room L-4296
San Ramon, CA 94583-2324
TimFinnigan@Chevron.com

Shihwei Liao
ConocoPhillips
OF 1084, T & MP
600 North Dairy Ashford
Houston, TX 77079
Shihwei.Liao@conocophillips.com

Finn Gunnar Nielsen
Norsk Hydro ASA
PO Box 7190
N-5020 Bergen, Norway

Street Address
Sandsliveien 90
N-5254 Sandsli, Norway

Finn.Gunnar.Nielsen@hydro.com

Kazuo Nishimoto
University of Sao Paulo
Department of Naval Architecture and Ocean Engineering
2231, Av. Prof. Mello Moraes
Cidade Universitaria
Sao Paulo, SP, Brazil CEPO05508-900
knishimo@usp.br

Stergios Liapis
Shell Oil Company
Offshore Structures
3737 Bellaire Blvd.
Houston, TX 77025
stergios.liapis@Shell.Com

Rick Mercier
Offshore Technology Research Center
1200 Mariner Drive
College Station, TX 77845-3400
rmercier@civil.tamu.edu

John Niedzwecki
Offshore Technology Research Center
1200 Mariner Drive
College Station, TX 77845-3400
j-Niedzwecki@.tamu.edu

Per Teigen
STATOIL
Postuttak
N 7005 Trondheim
Norway
pte@statoil.com

Street Address
Ark, Ebbels v.10
Rotvoll
Trondheim, Norway

John Letcher
AeroHydro
54 Herrick Road/PO Box 684
Southwest Harbor, ME 04679-0684
jletcher@aerohydro.com

Michael Shook
AeroHydro
54 Herrick Road/PO Box 684
Southwest Harbor, ME 04679-0684
mshook@aerohydro.com

Nick Newman
WAMIT
1 Bowditch Road
Woods Hole, MA 02543
jnn@mit.edu

Chang-Ho Lee
WAMIT
822 Boylston Street, Suite 202
Chestnut Hill, MA 02467
chlee@wamit.com

Sam Ryu
FMC Technologies Floating Systems
14741 Yorktown Plaza Dr.
Houston, TX 77040
sam.ryu@fmcti.com

Appendix

On the evaluation of quadratic forces on stationary bodies

Chang-Ho Lee
WAMIT Inc., Chestnut Hill MA, USA

October 15, 2006

Abstract. Conservation of momentum is applied to finite fluid volume surrounding a body and enclosed by the control surface in order to obtain expressions for all components of quadratic forces and moments acting on the body in terms of the momentum flux and the change of the momentum in the fluid volume. It is shown that the expressions derived are essentially identical with those obtained by a complementary approach in [1] where the pressure integrals on the body surface are tranformed into the integrals on the control surface using various vector theorems. Computational results are presented limited to the mean drift forces to illustrate the advantages of using control surfaces.

Keywords: control surface, mean drift force, momentum conservation, pressure integration, quadratic force

1. Introduction

The second-order quadratic forces contribute to the excitation at low or high frequencies than those of incident waves which may be important for the analysis of structures with certain resonance features such as moored vessels and Tension Leg Platforms. They are also important for the analysis of drift motion of vessels which can be of particular concern when the vessels operate in the proximity of other structures. For certain structures such as ships and spars, it is of interest to have accurate prediction of slowly varying roll and pitch loads.

The quadratic forces can be evaluated by the integration of fluid pressure over the instantaneous wetted surface as shown in [2], [3], [4] and [5]. As a special case, the horizontal mean drift force and vertical moment can also be evaluated from the momentum conservation principle applied to the entire volume of fluid as shown in [6] and [7]. Other than this special case, the computational result of the quadratic pressure forces is generally less accurate than that of the first order forces. Thus it requires significantly more refined descritization entailing increased computing time. This is because of the evaluation of the fluid velocity, which contributes to the quadratic forces, is less accurate than the pressure on the body surface. When the body has sharp corners, the quadratic pressure near the corner is singular, though integrable, and it

© 2006 *Kluwer Academic Publishers. Printed in the Netherlands.*

renders the computational result significantly inaccurate. Nonuniform discretization near the corner in the low order method [8], or nonuniform mapping in the higher order method [9] do produce more accurate results than otherwise. However the computational results can still be inaccurate especially when the bodies experience large motion.

In order to overcome this difficulty, Ferreira and Lee [10] applied momentum conservation over finite fluid volume surrounding the structures. All components of mean drift forces and moments on the body are obtained from the momentum flux through the control surface enclosing the fluid volume without the hydrodynamic pressure integration over the body surface. The computational results are significantly more accurate than the pressure integration. Recently Dai et al. [1] derived expressions for the quadratic forces and moments by transforming the pressure integration over the body surface into those on the control surface. One obvious advantage of these expressions is that the fluid velocity is not required on the body surface when body is fixed. Also the quadratic of the fluid velocity, which is most singular when body has sharp corners, in the pressure integration is not present in the new expressions having only linear terms in the fluid velocity.

In the following, we consider the conservation of momentum in the finite fluid volume surrounding a body and obtain the expressions for all components of quadratic forces and moments including complete mean drift forces and moments considered in [10]. It is shown that these expressions are equivalent to those obtained by a complementary approach in [1]. Computational results are presented for the mean drift forces to illustrate the advantage of present expressions.

2. Formulation

A potential flow is assumed which is governed by the velocity potential $\Phi(\vec{x}, t)$. The fluid pressure follows from Bernoulli's equation in the form

$$p(\vec{x}, t) = -\rho(\Phi_t + \frac{1}{2}\nabla\Phi \cdot \nabla\Phi + gz) \tag{1}$$

where ρ is the fluid density and g is gravity. $\vec{x} = (x, y, z)$ is the coordinates in a space-fixed Cartesian coordinate system with positive z pointing upward, perpendicular to the undisturbed free surface. t denotes time.

The forces on the body are then obtained from

$$\vec{F} = -\rho \iint_{s_b} \vec{n}[\Phi_t + \frac{1}{2}\nabla\Phi \cdot \nabla\Phi + gz]ds \tag{2}$$

and the moment from

$$\vec{M} = -\rho \iint_{s_b} (\vec{x} \times \vec{n})[\Phi_t + \frac{1}{2}\nabla\Phi \cdot \nabla\Phi + gz]ds \tag{3}$$

where $\vec{n}$ is unit normal vector pointing outward from the fluid domain and s_b denotes instantaneous wetted body surface.

The control volume considered is surrounded by s_b and by the control surface s_c. If s_b and s_c intersect the free surface, we denote the intersection as w and c, respectively. The free surface between w and c is denoted by s_f. It is assumed that s_b and s_c intersect the undisturbed free surface perpendicularly. The rate of change of the linear momentum **P** of the fluid in the control volume is

$$\frac{d\mathbf{P}(t)}{dt} = \rho\frac{d}{dt}\iiint \vec{V}dv = \rho \iint_{s_{bfc}} [\Phi_t\vec{n} + \nabla\Phi(\vec{U}\cdot\vec{n})]ds \tag{4}$$

and the rate of change of the angular momentum **H** is

$$\begin{aligned} \frac{d\mathbf{H}(t)}{dt} &= \rho\frac{d}{dt}\iiint(\vec{x}\times\vec{V})dv \\ &= \rho\iint_{s_{bfc}}[\Phi_t(\vec{x}\times\vec{n}) + (\vec{x}\times\nabla\Phi)(\vec{U}\cdot\vec{n})]ds \end{aligned} \tag{5}$$

Here $\vec{V}$ is the fluid velocity and $\vec{U}$ is the velocity of the control surface. Thus $\vec{U}\cdot\vec{n} = 0$ on s_c and $\vec{U}\cdot\vec{n} = \dfrac{\partial\Phi}{\partial n}$ on s_b and s_f.

Using an identity given in [11, p134]

$$\iint_{s_{bfc}} [\frac{\partial\Phi}{\partial n}\nabla\Phi - \frac{1}{2}(\nabla\Phi\cdot\nabla\Phi)\vec{n}]ds = 0 \tag{6}$$

and the equations (4) and (5), we have the force and moment in the forms

$$\begin{aligned} \vec{F} &= \rho\iint_{s_c}[(\Phi_t + \frac{1}{2}\nabla\Phi\cdot\nabla\Phi)\vec{n} - \frac{\partial\Phi}{\partial n}\nabla\Phi]ds \\ &+ \rho\iint_{s_f}(\Phi_t + \frac{1}{2}\nabla\Phi\cdot\nabla\Phi)\vec{n}ds - \rho g\iint_{s_b} z\vec{n}ds - \frac{d\mathbf{P}}{dt} \end{aligned} \tag{7}$$

and

$$\begin{aligned} \vec{M} &= \rho\iint_{s_c}[(\Phi_t + \frac{1}{2}\nabla\Phi\cdot\nabla\Phi)(\vec{x}\times\vec{n}) - \frac{\partial\Phi}{\partial n}(\vec{x}\times\nabla\Phi)]ds \\ &+ \rho\iint_{s_f}(\Phi_t + \frac{1}{2}\nabla\Phi\cdot\nabla\Phi)(\vec{x}\times\vec{n})ds \\ &- \rho g\iint_{s_b} z(\vec{x}\times\vec{n})ds - \frac{d\mathbf{H}}{dt} \end{aligned} \tag{8}$$

Considering quadratic terms from the foregoing equations as shown in Appendix, we have the expressions for the quadratic forces and moments. We first consider the mean drift forces and moments. Since the time averages of last terms in the equations (7) and (8) vanish, there is no contribution from these terms to the mean forces and moments. The force can be obtained from the time average of

$$\begin{aligned}\vec{F}^{(2)} = & -\frac{1}{2}\frac{\rho}{g}\int_C \vec{n}'\phi_t^2 dl - \rho g \int_W [\zeta(\vec{\Xi}\cdot\vec{n}')]\vec{k}dl \\ & -\rho\iint_{S_c}[\nabla\phi\frac{\partial\phi}{\partial n} - \frac{1}{2}\vec{n}(\nabla\phi\cdot\nabla\phi)]ds \\ & +\rho\vec{k}\iint_{S_f}(\zeta\frac{\partial\phi_t}{\partial z} + \frac{1}{2}\nabla\phi\cdot\nabla\phi)ds + \vec{F}_S^{(2)} \end{aligned} \quad (9)$$

and the moment from

$$\begin{aligned}\vec{M}^{(2)} = & -\frac{1}{2}\frac{\rho}{g}\int_C (\vec{x}\times\vec{n}')\phi_t^2 dl - \rho g \int_W \zeta(\vec{\Xi}\cdot\vec{n}')(\vec{x}\times\vec{k})dl \\ & -\rho\iint_{S_c}[(\vec{x}\times\nabla\phi)\frac{\partial\phi}{\partial n} - \frac{1}{2}(\vec{x}\times\vec{n})(\nabla\phi\cdot\nabla\phi)]ds \\ & +\rho\iint_{S_f}(\vec{x}\times\vec{k})(\zeta\frac{\partial\phi_t}{\partial z} + \frac{1}{2}\nabla\phi\cdot\nabla\phi)ds + \vec{M}_S^{(2)} \end{aligned} \quad (10)$$

Here ϕ denotes the first order velocity potential and $\zeta = -(1/g)\phi_t$ denotes the first order wave elevation. S_b, S_f and S_c are undisturbed body surface, free surface and control surface. W and C are the intersections of S_b and S_c with undisturbed free surface. $\vec{n}'$ denotes two dimensional normal vector to W and C on S_f, ∇' two dimensional gradient on S_f and $\vec{k}$ the unit vector in z. $\vec{\Xi} = (\Xi_1, \Xi_2, \Xi_3) = \vec{\xi} + \vec{\alpha}\times\vec{x}$ where $\vec{\xi}$ and $\vec{\alpha}$ denote the motion amplitudes of the translational and the rotational modes, respectively. Finally $\vec{F}_S^{(2)}$ and $\vec{M}_S^{(2)}$ denote parts of hydrostatic forces and moments and they are given in Appendix. We note above equations are different from those in [10].

The expressions for the quadratic forces and moments are completed by adding the quadratic terms of the changes of the linear momentum of the fluid volume

$$\begin{aligned}-\frac{d\mathbf{P}^{(2)}(t)}{dt} = & -\rho\iint_{S_f}[\nabla\phi\frac{\partial\phi}{\partial n} + \zeta\nabla\phi_t]ds \\ & -\rho\iint_{S_b}[\nabla\phi(\frac{d\vec{\Xi}}{dt}\cdot\vec{n}) + (\Xi\cdot\vec{n})\nabla\phi_t]ds \end{aligned} \quad (11)$$

and the angular momentum

$$-\frac{d\mathbf{H}^{(2)}(t)}{dt} = -\rho\iint_{S_f}\vec{x}\times[\nabla\phi\frac{\partial\phi}{\partial n} + \zeta\nabla\phi_t]ds$$

$$- \rho \iint_{S_b} \vec{x} \times [\nabla\phi(\frac{d\vec{\Xi}}{dt} \cdot \vec{n}) + (\Xi \cdot \vec{n})\nabla\phi_t]ds \quad (12)$$

to the equations (9) and (10). Among several expressions, (11) and (12) render the total forces and moments in the most compact forms. The derivations of these equations are provided in the Appendix. The final expressions for the quadratic forces and moments derived here are the same as those given in [1].

3. Numerical Results and Discussions

We first consider a hemisphere which is freely floating in infinite water depth. The incident wave travels to the positive x axis. Figure 1 shows the hemisphere enclosed by the cylindrical control surface. The radius of the sphere is 1 meter and the radius and draft of the control surface are 1.2 meters. Computations are made using the higher-order option of the panel program WAMIT. The geometry of the sphere and that of the control surface are represented analytically. A quadrant of the hemisphere is represented by a patch and a quadrant of the interior free surface of the hemisphere is also represented by a patch. The latter is introduced to eliminate the effect of the irregular frequencies. The unknown velocity potential on each patch is represented by quadratic B-splines. Each patch is subdivided into 1, 4 and 16 higher order panels to examine the convergence of the computational results. On the control surface, a fixed number of control points in the calculation of the momentum flux. The bottom, side and top of the cylindrical control surface are represented by 12, 12 and 4 subdivisions, respectively. The integration is carried out using 9 nodes Gauss quadrature on each subdivision assuming quadratic variation of the momentum flux. Thus 252 control points are used in total. The mean surge drift forces on the hemisphere are showed on the left column of Figure 3 which will be discussed below.

Next we consider a freely floating truncated circular cylinder of radius and draft 1 meters in infinite water depth. The center of rotation of the cylinder is at the intersection of the axis of the cylinder with the free surface while the center of gravity is 1 meter below the free surface. The radius of gyration of the pitch mode is 0.5 meters. Figure 2 shows the cylinder and the control surface. Three patches are used to represented the cylinder including the interior free surface and 3, 12 and 48 higher-order panels are used in the computation. The geometry of the cylinder is represented analytically with nonuniform mapping near the corner. As in the previous computation, 252 control points are used, in total, on the same cylindrical control surface of the radius and draft of 1.2 meters. The mean surge drift forces on the cylinder are showed on the right column of Figure 3.

Figure 3 shows the surge mean drift forces on the hemisphere on the left column and those on the cylinder on the right column. The computational results are more accurate toward the bottom plots for which finer discretization is used. Each plot contains three surge forces computed by three approaches; the pressure integration on the body surface [5], the far field momentum conservation [6] and the momentum conservation within the control surface. The figure shows the results from the pressure integration are least accurate. Specifically, while the mean surge force on the cylinder, which has a sharp corner, can be calculated accurately using 3 panels up to around $KR = 3$ by momentum conservation, it is necessary to use 48 panels for the pressure integration. Since the computational time for the linear solution in the higher-order method is typically proportional to the square of the number of panels, the momentum conservation can be orders of magnitude more efficient than the pressure integration for the evaluation of the mean forces. The figure also shows the results using the control surface are identical with those from the momentum conservation to the graphical accuracy. The computational time using the control surface depends on the number of control points. Using compact control surfaces surrounding the body, as shown in this example, the additional computating time for the calculation of the momentum flux on the control surface can be similar to that for the linear solution.

This example illustrates the advantages of using control surface for the calculation of mean forces. The computational results are as accurate as those from the far field momentum conservation. All components of mean forces and moments can be calculated more efficiently than the pressure integration. For multiple bodies, the forces and moments on individual body can be obtained using separate control surface surrounding each body which is not possible by the far field momentum conservation.

4. Conclusion

We derived expressions for the quadratic forces and moments by applying momentum conservation in the finite volume surrounding the body. The final form of the expressions can be made to be identical to those obtained by Dai et al. [1]. Computations of mean drift forces show the accuracy and efficiency of using the control surfaces. All components of the forces and moments can be evaluated as with the pressure

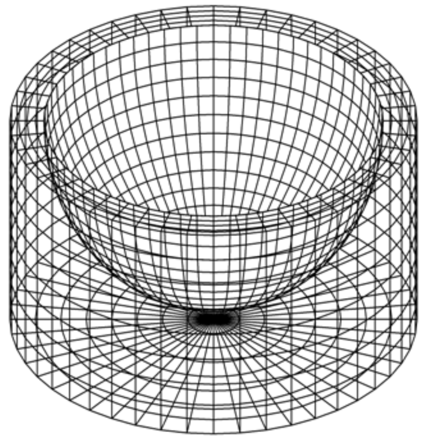

Figure 1. Geometry of the hemisphere and control surface. The radius of the sphere is 1. The radius and draft of the cylindrical control surface are 1.2. The meshes are for the purpose of the visualization only.

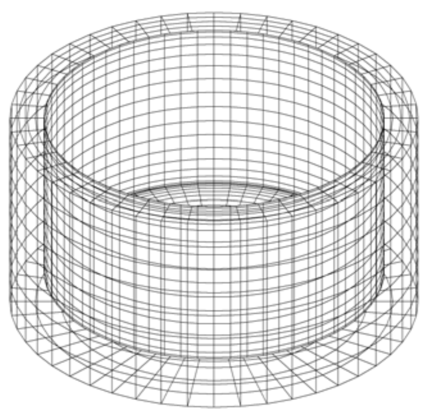

Figure 2. Geometry of the cylinder and control surface. The radius and draft of the cylinder are 1. The radius and draft of the cylindrical control surface are 1.2. The meshes are for the purpose of the visualization only.

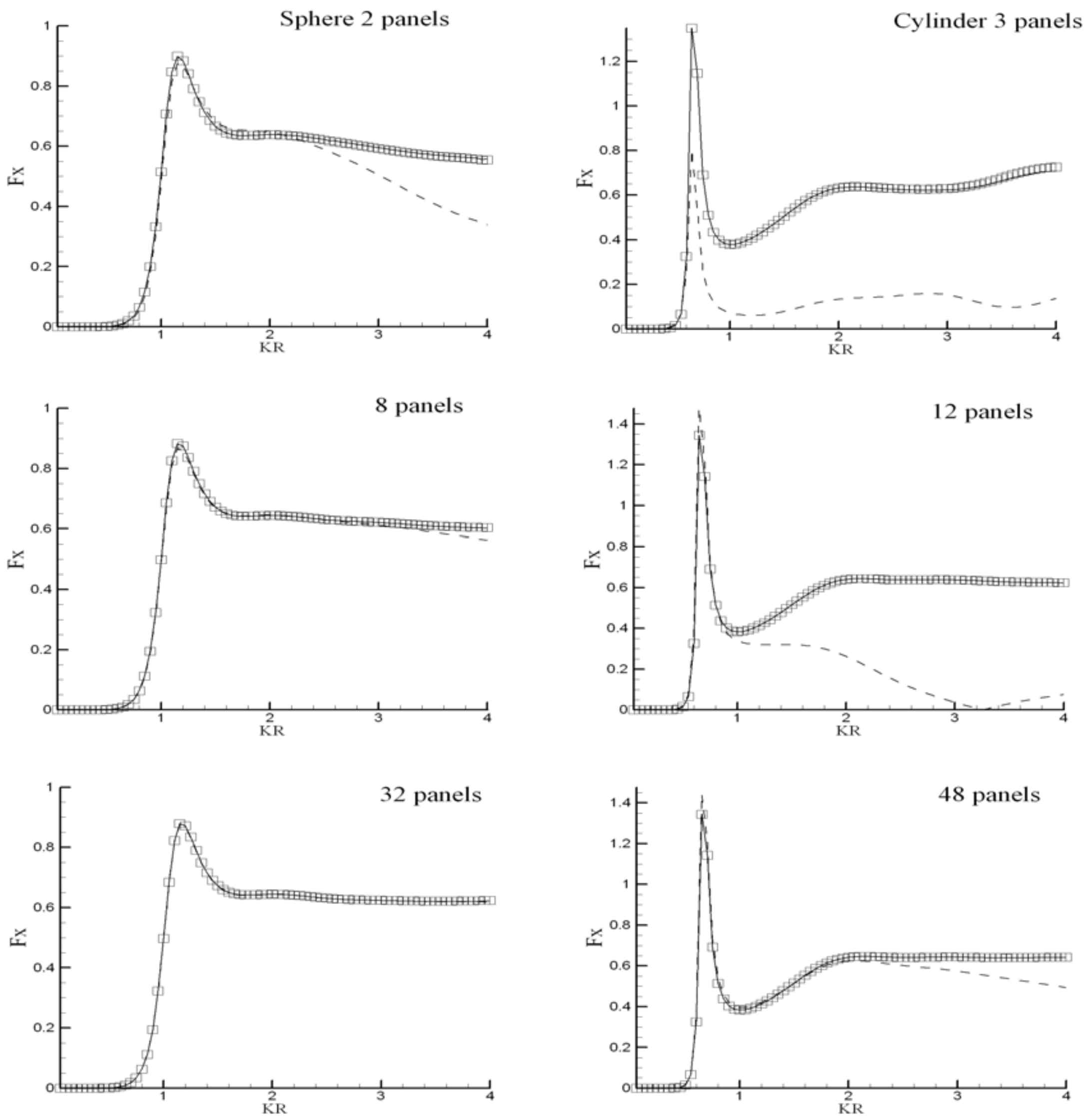

Figure 3. Nondimensional mean surge forces on the hemisphere and cylinder. The forces on the hemisphere is on the left column and those on the cylinder on the right column. The forces are normalized by $\rho g R A^2$ where ρ is the water density, g is the gravitational acceleration, R is the radius and A is the wave amplitude. K is the infinite depth wave number. Forces by the pressure integration are represented by dashed lines, those by the momentum conservation by solid lines and those by using control surface are represented by squares.

integration but by avoiding the integration of pressure on the body the computational results are as accurate as the far field momentum conservation.

The expressions for the quadratic forces and moments in bichromatic waves contain the integration over the body surface of the pressure proportional to the fluid velocity, as shown in the equations (11) and (12). Thus further study is needed to find the computational advantage of the current approach, in particular, when the body has sharp corners. However, in comparison with the pressure integration, the pressure to be integrated is less singular. In addition, when low frequency forces are of interest, the contribution from the integration over the body surface will be small, linearly proportional to the difference of two frequencies.

Appendix

The quadratic terms of the integral on s_c, denoted by F_{S_c}, are given in the form

$$\vec{F}^{(2)}_{S_c} = -\frac{\rho}{g}\int_C \vec{n}'\phi_t^2 dl - \rho\iint_{S_c}[\nabla\phi\frac{\partial\phi}{\partial n} - \frac{1}{2}\vec{n}(\nabla\phi\cdot\nabla\phi)]ds \quad (13)$$

where the first line integral accounts for the momentum flux over the portion of s_c for $z = (0, \zeta)$.

The quadratic terms of the integral on s_f, denoted by F_{S_f}, are

$$\begin{aligned}\vec{F}^{(2)}_{S_f} = &- \rho g\vec{k}\int_W [\zeta(\vec{\Xi}\cdot\vec{n}')]dl + \frac{\rho\vec{k}}{2}\iint_{S_f}(\nabla\phi\cdot\nabla\phi)ds \\ &+ \frac{\rho}{g}\iint_{S_f}\phi_t\nabla'\phi_t ds + \rho\vec{k}\iint_{S_f}\zeta\frac{\partial\phi_t}{\partial z}ds \qquad (14)\end{aligned}$$

where the first line integral accounts for the vertical momentum flux over the portion of free surface between the mean position of the waterline W and the unsteady line of intersection of the body with the free surface w. The third integral accounts for the horizontal momentum flux due to the slope of the free surface elevation. This term was omitted in the equation (13) of [10]. The last integral is due to the expansion of the velocity potential from S_f to ζ.

The quadratic terms due to the hydrostatic pressure on s_b are obtained by two integrals. One is over the mean wetted body surface S_b and the result, following [5], takes a form

$$\begin{aligned}\vec{F}^{(2)}_{S_b} &= -\rho g\iint_{S_b} z\vec{n}ds \\ &= \vec{\alpha}\times(-\rho g A_{wp}(\xi_3 + \alpha_1 y_f - \alpha_2 x_f)\vec{k}) + F^{(2)}_S \qquad (15)\end{aligned}$$

where A_{wp} is the waterplane area, x_f and y_f are the coordinates of the center of floatation and

$$F_S^{(2)} = -\rho g A_{wp}[\alpha_1\alpha_3 x_f + \alpha_2\alpha_3 y_f + \frac{1}{2}(\alpha_1^2+\alpha_2^2)Z_o]\vec{k} \qquad (16)$$

Here Z_o denotes the vertical coodinate of the origin of the body-fixed coordinates system relative to the mean free surface.

The second integral is over the region between $z = \Xi_3$ and $z = \zeta$ on s_b and it takes the form

$$\vec{F}_W^{(2)} = -\rho g \int_W dl \int_0^{\zeta-\Xi_3} (\bar{z}+\Xi_3)\vec{n} d\bar{z} = -\frac{1}{2}\rho g \int_W \vec{n}'(\zeta^2 - \Xi_3^2) dl \quad (17)$$

where the vertical coordinate of the body fixed coordinates system $\bar{z} = z - \Xi_3$.

Invoking Stoke's theorem to a vector $\vec{V}$, we have a relation

$$\int\!\!\int [(\vec{n}\times\nabla)\times\vec{V}]ds = \int(\vec{t}\times\vec{V})dl = -\int[V_3\vec{n}' - (\vec{V}\cdot\vec{n}')\vec{k}]dl \quad (18)$$

when the tangential vector t in the line integral is perpendicular to $\vec{k}$ Applying this relation over the region enclosed by the waterline, W with $\vec{V} = (0,0,\Xi_3^2)$, we have

$$\frac{1}{2}\rho g \int_W (\vec{n}'\Xi_3^2) dl = \vec{\alpha}\times(\rho g A_{wp}(\xi_3 + \alpha_1 y_f - \alpha_2 x_f)\vec{k}) \qquad (19)$$

Similarly, applying this relation between W and C with $\vec{V} = (0,0,\zeta^2)$, we have

$$\frac{1}{2}\rho g(\int_W \vec{n}'\zeta^2 dl + \int_C \vec{n}'\zeta^2 dl) = \frac{\rho}{g}\int\!\!\int_{S_f} \phi_t \nabla'\phi_t ds \qquad (20)$$

Excluding the change of momentum $d\mathbf{P}/dt$, the quadratic forces can be obtained as the sum of $\vec{F}_{S_c}^{(2)}, \vec{F}_{S_f}^{(2)}, \vec{F}_{S_b}^{(2)}$ and $\vec{F}_W^{(2)}$. Upon substituting the relations in the equations (19) and (20) to this sum, we have the mean forces in the form shown in the equation (9). The expression for the moments can be obtained in the similar manner and it is shown in the equation (10). Here we provide the hydrostatic moments, $M_S^{(2)}$, for the completeness.

$$\begin{aligned} M_S^{(2)} &= \rho g\{[-A_{wp}(\xi_3\alpha_3 x_f + \frac{1}{2}(\alpha_1^2+\alpha_2^2)Z_o y_f) - 2\alpha_1\alpha_3 L_{12} \\ &+ \alpha_2\alpha_3(L_{11} - L_{22}) + \forall(\alpha_1\alpha_2 x_b - \frac{1}{2}(\alpha_1^2+\alpha_3^2)y_b)] \\ &- A_{wp}(\xi_3 + \alpha_1 y_f - \alpha_2 x_f)(\alpha_1 Z_o + \xi_2)\}\vec{i} \end{aligned}$$

$$
\begin{aligned}
&+ \ \rho g\{[-A_{wp}(\xi_3\alpha_3 y_f - \frac{1}{2}(\alpha_1^2+\alpha_2^2)Z_o x_f) + 2\alpha_2\alpha_3 L_{12} \\
&+ \ \alpha_1\alpha_3(L_{11}-L_{22}) + \forall\frac{1}{2}(\alpha_2^2+\alpha_3^2)x_b)] \\
&- \ A_{wp}(\xi_3+\alpha_1 y_f - \alpha_2 x_f)(\alpha_2 Z_o - \xi_1)\}\vec{j} \qquad (21)
\end{aligned}
$$

where $\forall$ denotes the volume of the body and x_b and y_b are the coordinates of the center of buoyancy. L_{ij} denotes the moments of the waterplane area with the subscript i and j corresponding to the x and y coordinates.

We next consider the quadratic terms due to the change of momentum inside the control volume in the equations (4) and (5). The quadratic term of the integral on s_c vanishes except over the region $z=(0,\zeta)$. Those on s_b and s_f can be expressed in terms of the integrals over the mean surfaces, S_b and S_f. Invoking Stoke's theorem on S_b and using the vector relations given in [12, Chapter 6, equations (74d) and (74e)], we have following two relations, one for the linear momentum

$$
\begin{aligned}
&g\int_W \zeta[(\Xi_3\vec{n}' - (\vec{\Xi}\cdot\vec{n}')\vec{k}]dl \ + \ \alpha\times\iint_{S_b}\phi_t\vec{n}ds \\
&\qquad = \iint_{S_b}[(\Xi\cdot\vec{n})\nabla\phi_t \ - \ \vec{n}(\vec{\Xi}\cdot\nabla\phi_t)]ds \qquad (22)
\end{aligned}
$$

and the other for the angular momentum

$$
\begin{aligned}
&g\int_W \zeta\vec{x}\times[\Xi_3\vec{n}' - (\vec{\Xi}\cdot\vec{n}')\vec{k}]dl \ + \ \vec{\xi}\times\iint_{S_b}\phi_t\vec{n}ds + \vec{\alpha}\times\iint_{S_b}(\vec{x}\times\vec{n})\phi_t ds \\
&\qquad = \iint_{S_b}[(\Xi\cdot\vec{n})(\vec{x}\times\nabla\phi_t) \ - \ (\vec{x}\times\vec{n})(\vec{\Xi}\cdot\nabla\phi_t)]ds \qquad (23)
\end{aligned}
$$

Using above relations, it can be shown that the changes of momentum in (4) and (5) take the forms

$$
\begin{aligned}
\frac{d\mathbf{P}^{(2)}(t)}{dt} \ &= \ \rho\iint_{S_f}[\nabla\phi\frac{\partial\phi}{\partial n} + \zeta\nabla\phi_t]ds \\
&+ \ \rho\iint_{S_b}[\nabla\phi(\frac{d\vec{\Xi}}{dt}\cdot\vec{n}) + (\Xi\cdot\vec{n})\nabla\phi_t]ds \qquad (24)
\end{aligned}
$$

and

$$
\begin{aligned}
\frac{d\mathbf{H}^{(2)}(t)}{dt} \ &= \ \rho\iint_{S_f}\vec{x}\times[\nabla\phi\frac{\partial\phi}{\partial n} + \zeta\nabla\phi_t]ds \\
&+ \ \rho\iint_{S_b}\vec{x}\times[\nabla\phi(\frac{d\vec{\Xi}}{dt}\cdot\vec{n}) + (\Xi\cdot\vec{n})\nabla\phi_t]ds \qquad (25)
\end{aligned}
$$

References

[1] Dai, Y.-S., Chen, X.-B. and W.-Y. Duan Computation of Low-Frequency Loads by the Middle-Field Formulation. J. Grue (ed) *20th Workshop for Water Waves and Floating Bodies*, 47–50, Longyearbyen, Norway, 2005.

[2] Pinkster, J. A. Low frequency second-order exciting forces on floating structures. *NSMB report 650*, 1980.

[3] Ogilvie, T. F. Second-order hydrodynamic effects on ocean platforms. R.W. Young (ed), *International Workshop on Ship and Platform Motions*, Berkeley, CA, 1983.

[4] Molin, B. and J.-P. Hairault On Secon-Order Motion and Vertical Drift Forces for Three-Dimensional Bodies in Regular Waves. R.W. Young (ed), *International Workshop on Ship and Platform Motions*, Berkeley, CA, 1983.

[5] Lee, C.-H. and J. N. Newman First- and Second-order Wave Effects on a Submerged Spheroid. *Journal of Ship Research*, 35:183–190, 1991.

[6] Maruo, H. The Drift of a Body Floating on Waves. *Journal of Ship Research*, 4:1–10, 1960.

[7] Newman, J. N. The Drift Force and Moment on Ships in Waves. *Journal of Ship Research*, 11:51–60, 1967.

[8] Lee, C.-H. and J. N. Newman Sensitivity of Wave Load to the Discretization of Bodies. *Proceedings of Behaviour of Offshore Structures*, London, 1992.

[9] Lee, C.-H., Farina L., and J. N. Newman A Geometry-Independent Higher-Order Panel Method and its Application to WaveBody Interactions. E.O. Tuck, J.A.K. Stott (eds) *Proceedings of Engineering Mathematics and Applications Conference*, 303–306, Adelaide, Australia, 1998.

[10] Ferreira, M. D. and C.-H. Lee Computation of Second-Order Mean Wave Forces and Moments in Multibody Interaction. C. Chryssostomidis (ed) *Proceedings of Behaviour of Offshore Structures*, 2:303–313, Cambridge, MA, 1994.

[11] Newman, J. N. Marine Hydrodynamics. The MIT Press, 1980.

[12] Hildebrand, F. B. Advanced Calculus for Engineers. Prentice-Hall, 1976.